
Expert-Agnostic Learning to Defer

Joshua Strong, Prमित Saha, Yasin Ibrahim, Cheng Ouyang, Alison Noble
Department of Engineering Science, University of Oxford

Abstract

Learning to Defer (L2D) trains autonomous systems to handle straightforward cases while deferring uncertain ones to human experts. Recent advancements in this field have introduced methods that offer flexibility to unseen experts at test time. However, we find these approaches struggle to generalise to experts with behaviours not seen during training, require extensive human annotation, and lack mechanisms for incorporating prior knowledge of expert capabilities. To address these challenges, we introduce Expert-Agnostic Learning to Defer (EA-L2D), a novel L2D framework that employs a Bayesian approach to model expert behaviour in an *expert-agnostic* fashion. Across benchmark medical imaging datasets (HAM10000, Blood Cells, Retinal OCT, and Liver Tumours), EA-L2D significantly outperforms prior methods on unseen experts, achieving up to a 28% relative improvement, while also matching or exceeding state-of-the-art performance on seen experts.

1 Introduction

The practical implementation of AI in decision-sensitive environments often involves a delicate trade-off between the benefits of autonomy and the consequences of errors. Learning to Defer (L2D) [1] addresses this by training an AI system to autonomously handle straightforward cases whilst deferring challenging ones to human experts. This strategy is particularly useful in high-stakes domains such as healthcare, where deferral mitigates the risk of errors impacting patient safety.

Whilst the L2D field has seen many recent advancements, effectively adapting to *unseen* experts at test time remains a significant challenge. L2D-Pop [2] pioneered adapting L2D systems to unseen experts, predicting deferral decisions by conditioning on meta-learned implicit *latent* representations inferred from few-shot *context predictions* of the test-time expert. This approach learns fine-grained behavioural embeddings, enabling tailored deferral strategies for a population of experts. However, despite its notable strengths in tackling this task, we identify critical limitations motivating our work: (1) potential difficulties generalising to out-of-distribution (OOD) experts whose capabilities differ significantly from those encountered during meta-training, (2) the requirement for extensive expert annotations, and (3) the lack of mechanisms to incorporate prior knowledge about expert capabilities.

To address these limitations, we develop **Expert-Agnostic Learning to Defer (EA-L2D)** by approaching the objective from an alternative perspective. Unlike methods learning latent expert embeddings, EA-L2D *constructs* an explicit, interpretable Bayesian representation of expert performance from their *context predictions*. Deferral decisions are made by a rejector network comparing classifier outputs with key statistics from this representation. We term EA-L2D “expert-agnostic” because its deferral logic is learned based on the *structural relationship* between classifier confidence and quantified expert performance metrics (e.g., estimated accuracy and uncertainty at relevant classes), rather than being tied to specific expert identities or the nominal labels of their expertise classes. We demonstrate both theoretically and empirically that this focus on relative statistical competence, allows EA-L2D to generalise more robustly to OOD experts, even if their specialisations involve classes unseen during training. Furthermore, its Bayesian formulation enables additional benefits, in the incorporation of prior knowledge of expert’s and significantly reduces expert annotation requirements required for training.

To evaluate the effectiveness of EA-L2D, we conduct experiments on four diverse medical imaging datasets: HAM10000, Blood Cells, Retinal OCT, and Liver Tumours. We address three research questions: (1) *How does EA-L2D compare to state-of-the-art methods, particularly in terms of robustness to unseen experts and varying expert diversity?*, (2) *How does performance scale with experts possessing multiple areas of expertise?*, and (3) *What is the effect of incorporating prior knowledge, especially under limited context data?* Our results show that EA-L2D consistently outperforms prior methods, notably achieving up to a 28% relative improvement in deferral performance when encountering OOD experts. In summary, the main contributions of this work are:

1. We introduce EA-L2D, whose expert-agnostic deferral strategy significantly improves robustness to out-of-distribution experts, matching or exceeding prior SOTA on in-distribution cases, whilst enjoying a simpler and more computationally efficient implementation.
2. EA-L2D enables the optional incorporation of prior knowledge of expert capabilities, further boosting accuracy in low or no-context settings.
3. Additionally, EA-L2D offers a practical advantage by removing the requirement for expert annotations on training images, substantially reducing annotation costs.

2 Related Literature

Learning to Defer (L2D) The L2D paradigm [1] extends Rejection Learning [3, 4] by including human expert predictions into deferral decisions. L2D aims to learn a joint decision system that integrates deferral while maintaining Bayesian optimality. Since its introduction several extensions have emerged, including for multiple experts [5, 6], frameworks handling limited expert annotations [7–9], approaches that complement rather than defer to humans [10], methods for managing expert workload [8, 9], and two-stage systems that train classifiers and rejectors separately [11, 12]. L2D has seen application in healthcare [13, 14], fraud detection [15], and content moderation [16].

Learning to Defer to a Population Our approach to handling unseen experts at test time aligns in objective with the work of L2D-Pop [2], which uses meta-learning via Attentive Neural Processes [17] to adapt using *context predictions* (a few examples illustrating expert behaviour). However, the representation strategies diverge fundamentally. L2D-Pop *learns* a holistic, implicit latent vector. In contrast, EA-L2D *constructs* an explicit, structured Bayesian representation \mathcal{R}^E (§4.1) by quantifying class-specific performance. This yields two key benefits. First, EA-L2D’s deferral logic (§4.3) draws directly from relevant metrics in \mathcal{R}^E , such as estimated accuracy and uncertainty for key classes. By operating on these statistical relationships rather than learning associations tied to specific class identities or expert profiles, the resulting expert-agnostic mechanism (§A.2) generalises more robustly to OOD experts—unlike latent embeddings, which we find can overfit to training profiles (§5.4). Second, its Bayesian formulation naturally incorporates prior knowledge (§4.2), essential under data scarcity, whereas L2D-Pop defaults to a marginal model when context is absent. While meta-learning may be framed in Bayesian terms [18], the practical implications for representation, OOD generalisation, and prior use differ markedly. EA-L2D offers these advantages without complex meta-learning. A detailed comparison is provided in App A.1.

L2D with Limited Expert Predictions Our work also relates to L2D frameworks addressing limited expert predictions. Methods like Alves et al. [9] model expertise but may require unrealistic annotation levels. Anonymous [8] uses a probabilistic framework with Expectation-Maximisation to infer missing expert annotations as latent variables, enabling training with incomplete data. Hemmer et al. [7] trains an embedding model with an expertise predictor to generate artificial expert predictions. In contrast, our approach reduces reliance on complete annotations without auxiliary prediction models. Crucially, it generalises to previously unseen experts, enabling adaptation at test time. This data efficiency is further enhanced by incorporating prior expert knowledge at inference—a capability, to the best of our knowledge, novel amongst existing L2D methods.

Agnosticism in Machine Learning EA-L2D aligns with agnostic learning paradigms prioritising adaptability. For instance, MAML [19] learns a transferable initialisation adaptable to new tasks, while TAML [20] promotes unbiased models generalisable across tasks. Similarly, Agnostic Federated Learning [21] optimises a central model for any mixture of client distributions, enhancing fairness and robustness to distributional shifts. In the same spirit, EA-L2D learns a transferable *deferral evaluation function* (r_ϕ) based on statistical comparison, enabling broad applicability across expert profiles defined by \mathcal{R}^E , regardless of their class specialisations.

3 Background: Learning to Defer

Setup In a classification task, we predict a target $y \in \mathcal{Y} = \{1, \dots, K\}$ from inputs $\mathbf{x} \in \mathcal{X}$, where $(\mathbf{x}, y) \sim \mathcal{P}$. The Learning to Defer (L2D) framework assumes an expert E provides predictions $m \in \mathcal{M} = \mathcal{Y}$. Given a dataset $\mathcal{D} = \{(\mathbf{x}_i, y_i, m_i)\}_{i=1}^N$, the objective is to learn a predictor $\hat{Y} : \mathcal{X} \rightarrow \mathcal{Y} \cup \{\perp\}$ (\perp denotes deferral) by jointly training a *classifier* $h : \mathcal{X} \rightarrow \mathcal{Y}$ and a *rejector* $r : \mathcal{X} \rightarrow \{0, 1\}$. h predicts the target; r decides to use $h(\mathbf{x})$ ($r(\mathbf{x}) = 0$) or defer ($r(\mathbf{x}) = 1$).

Optimisation Assuming costs $l(\mathbf{x}, y, h(\mathbf{x}))$ for classification and $l_{\text{exp}}(\mathbf{x}, y, m)$ for deferral, the system loss is:

$$\mathcal{L}(h, r) = \mathbb{E}_{(\mathbf{x}, y) \sim \mathcal{P}, m \sim M | (\mathbf{x}, y)} \left[l(\mathbf{x}, y, h(\mathbf{x})) \mathbb{I}_{r(\mathbf{x})=0} + l_{\text{exp}}(\mathbf{x}, y, m) \mathbb{I}_{r(\mathbf{x})=1} \right]. \quad (1)$$

This non-convex loss $\mathcal{L}(h, r)$ is hard to optimise directly; Mozannar and Sontag [22] proposed a consistent surrogate for Eq. (1), derived from the Bayes minimiser of the 0-1 system loss. The 0-1 loss is:

$$\mathcal{L}_{0-1}(h, r) = \mathbb{E}_{(\mathbf{x}, y) \sim \mathcal{P}, m \sim M | (\mathbf{x}, y)} \left[\mathbb{I}_{h(\mathbf{x}) \neq y} \mathbb{I}_{r(\mathbf{x})=0} + \mathbb{I}_{m \neq y} \mathbb{I}_{r(\mathbf{x})=1} \right].$$

Minimising \mathcal{L}_{0-1} yields the Bayes-optimal classifier $h^*(\mathbf{x})$ and rejector $r^*(\mathbf{x})$:

$$h^*(\mathbf{x}) = \arg \max_{y \in \mathcal{Y}} \mathbb{P}(\mathcal{Y} = y | \mathcal{X} = \mathbf{x}), \quad r^*(\mathbf{x}) = \mathbb{I} \left[\mathbb{P}(\mathcal{Y} = \mathcal{M} | \mathcal{X} = \mathbf{x}) \geq \max_{y \in \mathcal{Y}} \mathbb{P}(\mathcal{Y} = y | \mathcal{X} = \mathbf{x}) \right].$$

With score functions $g_y(\mathbf{x})$ for $h(\mathbf{x}) = \arg \max_y g_y(\mathbf{x})$ and $g_{\perp}(\mathbf{x})$ for $r(\mathbf{x}) = \mathbb{I}[\max_y g_y(\mathbf{x}) \leq g_{\perp}(\mathbf{x})]$, a consistent softmax-based surrogate is:

$$\mathcal{L}_{CE}(g_1, \dots, g_K, g_{\perp}; \mathbf{x}, y, m) = -\log P(y | \mathbf{x}) - \mathbb{I}[m = y] \log P(\perp | \mathbf{x}), \quad (2)$$

where $P(y' | \cdot) = \exp\{g_{y'}(\cdot)\} / \sum_{y'' \in \mathcal{Y} \cup \{\perp\}} \exp\{g_{y''}(\cdot)\}$. This loss encourages accurate classification (via g_y) and deferral (via g_{\perp}) when the expert is correct ($m = y$). At inference, prediction is deferred if $g_{\perp}(\mathbf{x}) \geq \max_{y \in \mathcal{Y}} g_y(\mathbf{x})$.

4 Methodology: Expert-Agnostic Learning to Defer

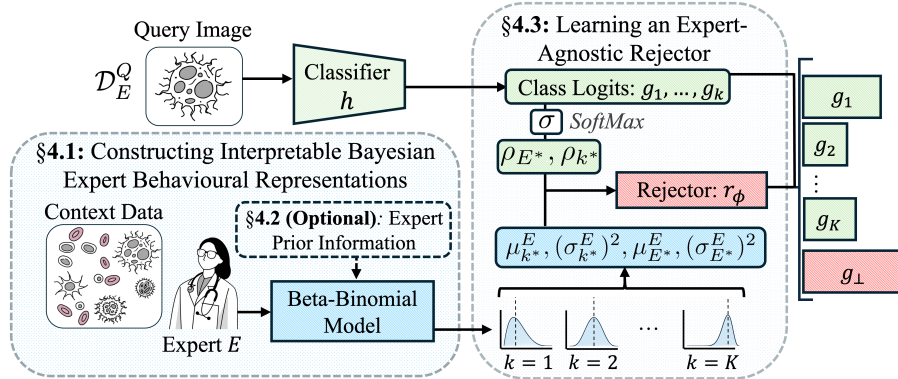


Figure 1: Overview of Expert-Agnostic Learning to Defer (EA-L2D). An arbitrary expert E 's context data \mathcal{D}_C^E is modelled (Beta-Binomial, §4.1) into a behavioural representation \mathcal{R}^E (class-wise posterior means/variances), with optional priors (§4.2). EA-L2D's expert-agnostic rejector (§4.3) compares classifier outputs against \mathcal{R}^E . This 'agnosticism' (operating without dependence on specific expert identities or known specialisms) enables robust generalisation to diverse and unseen experts, a key advantage over methods that learn profiles tied to training-time experts.

In this section, we introduce Expert-Agnostic Learning to Defer (EA-L2D). Our method is structured as follows: constructing interpretable Bayesian expert representations (§4.1), incorporating known expertise as priors (§4.2), learning an expert-agnostic deferral (§4.3), and optimising under uncertainty with reduced annotations (§4.4). Fig. 1 provides an overview, and Alg. 1 details the procedure.

Setup For each expert E , we assume a *context dataset* $\mathcal{D}_C^E = \{\mathbf{x}_i^C, y_i^C, m_{i,E}^C\}_{i=1}^{N_C^E}$ to estimate expert behaviour (e.g., historical predictions) and a *query dataset* $\mathcal{D}_Q = \{\mathbf{x}_i^Q, y_i^Q\}_{i=1}^{N_Q}$ for learning deferral. We assume $N_C^E \ll N_Q$ and $\mathcal{D}_C^E \cap \mathcal{D}_Q = \emptyset$. N_C^E can vary per expert, while N_Q is fixed.

4.1 Constructing Interpretable Bayesian Expert Behavioural Representations

EA-L2D constructs an explicit and interpretable behavioural representation \mathcal{R}^E for arbitrary expert E from context data \mathcal{D}_C^E by modelling the expert’s accuracy for each class $k \in \mathcal{Y}$ with a Beta distribution. This approach leverages the Beta-Binomial conjugate model, which arises naturally when using a Binomial likelihood for the observed correct predictions within \mathcal{D}_C^E . We provide further motivation for the Beta-Binomial model in App. A.1.

Let n_k be the count of class k samples in \mathcal{D}_C^E , and t_k^E be the count of correct predictions made by E for these samples. We model the expert’s unknown accuracy θ_k^E for class k using a Beta distribution. With a uniform prior $\theta_k^E \sim \text{Beta}(1, 1)$, the posterior distribution after observing the context data is:

$$\theta_k^E | \mathcal{D}_C^E \sim \text{Beta}(\alpha_k, \beta_k), \quad \text{where } \alpha_k := 1 + t_k^E, \beta_k := 1 + n_k - t_k^E.$$

While the posterior distribution is fully defined by its parameters α_k and β_k , we utilise the posterior mean and variance for a more interpretable representation:

$$\mu_k^E := \mathbb{E}[\theta_k^E | t_k^E, n_k] = \frac{1 + t_k^E}{2 + n_k}, \quad (\sigma_k^E)^2 := \text{Var}[\theta_k^E | t_k^E, n_k] = \frac{(1 + t_k^E)(1 + n_k - t_k^E)}{(2 + n_k)^2(3 + n_k)}.$$

Here, μ_k^E represents the expected accuracy of expert E on class k , and the variance $(\sigma_k^E)^2$ quantifies the uncertainty associated with this estimate. The expert’s primary *expertise class* is identified by the greatest posterior mean: $E^* := \arg \max_{k \in \mathcal{Y}} \mu_k^E$. The complete behavioural representation \mathcal{R}^E then comprises a vector capturing the mean accuracy and associated uncertainty for every class: $\mathcal{R}^E := [(\mu_{k=1}^E, (\sigma_{k=1}^E)^2), \dots, (\mu_{k=K}^E, (\sigma_{k=K}^E)^2)] \in ([0, 1] \times [0, 0.25])^K$. During training, \mathcal{R}^E is computed dynamically per batch of data. For each expert E , we sample a context subset d_E^C of size $n_C^E \subset N_C^E$ from \mathcal{D}_C^E (Alg. 1, Line 5) and calculate \mathcal{R}^E from this subset. This trains the rejector to account for the sampling variability in estimating expert performance.

To ensure that the model reliably identifies the expert’s strongest class, we establish conditions under which the class corresponding to the maximal true accuracy is selected with high probability. The following result provides both an asymptotic guarantee and a finite-sample bound.

Proposition 1. *Let K be the number of classes, and suppose each expert E has true but unknown per-class accuracies $\bar{\theta}_k^E \in [0, 1]$. Let $k^* \in \mathcal{Y}$ be the unique class of maximal expertise, such that $\bar{\theta}_{k^*}^E > \bar{\theta}_k^E$ for all $k \neq k^*$. Then, as the number of context samples $n_k \rightarrow \infty$ for each class k , the posterior mean estimates μ_k^E converge almost surely to $\bar{\theta}_k^E$, and the selected expertise class $\arg \max_k \mu_k^E$ converges almost surely to k^* . Moreover, if each class k is observed at least n times, where*

$$n \geq \frac{\ln(\frac{2K}{\delta})}{2(\frac{\Delta}{2})^2}, \quad \text{with } \Delta := \bar{\theta}_{k^*}^E - \max_{k \neq k^*} \bar{\theta}_k^E,$$

then with probability at least $1 - \delta$, the posterior means satisfy $\mu_{k^}^E > \mu_k^E$ for all $k \neq k^*$; that is, the correct expertise class is identified. Proof: See App. C.1.*

4.2 Incorporating Known Expertise as Priors

EA-L2D enables the optional incorporation of prior knowledge regarding an expert’s capabilities to further inform the behavioural representation \mathcal{R}^E . This is particularly useful when context data \mathcal{D}_C^E is sparse. If an expert provides a self-assessed accuracy p_k^E and confidence $c_k^E \in [0, 1]$ for class k , these can be used to set the Beta prior parameters $(\alpha_k^{\text{prior}}, \beta_k^{\text{prior}})$:

$$\alpha_k^{\text{prior}} := 1 + c_k^E p_k^E (s - 2), \quad \beta_k^{\text{prior}} := 1 + c_k^E (1 - p_k^E) (s - 2),$$

where the prior strength $s \geq 2$ controls the prior’s influence relative to the context data. We recommend $s = 10$ for moderate influence. Low confidence $c_k^E \approx 0$ yields a near-uniform prior Beta(1, 1), whereas higher confidence integrates the assessment more strongly.

While informative priors can improve data efficiency, they risk being misspecified if the expert’s self-assessment p_k^E is inaccurate relative to their true performance. A key benefit of the Bayesian framework is that the posterior estimate of the expert’s accuracy still converges to the true value as more context data n_k is observed, irrespective of the initial prior (Proposition 1). However, a natural question is: *how much data is required to overcome a potentially inaccurate prior?* The following proposition provides a lower bound:

Proposition 2 (Sample Complexity for Overcoming Prior Misspecification). *Let $\bar{\theta}_k^E$ be the true accuracy of expert E for class k , with prior $\text{Beta}(\alpha_k^{\text{prior}}, \beta_k^{\text{prior}})$ having mean μ_{prior} and strength $S_{\text{prior}} = \alpha_k^{\text{prior}} + \beta_k^{\text{prior}}$. For any $\epsilon > 0$ and $\delta \in (0, 1)$, the number of context samples n_k needed to ensure the posterior mean μ_k^E satisfies $|\mu_k^E - \bar{\theta}_k^E| < \epsilon$ with probability at least $1 - \delta$ is bounded by:*

$$n_k \geq \max \left\{ \frac{S_{\text{prior}}(|\mu_{\text{prior}} - \bar{\theta}_k^E| - \epsilon/2)}{\epsilon/2}, \frac{2 \ln(2/\delta)}{\epsilon^2} \right\}$$

The first term accounts for overcoming prior bias (relevant if $|\mu_{\text{prior}} - \bar{\theta}_k^E| > \epsilon/2$) and the second accounts for statistical uncertainty via Hoeffding’s inequality. Proof: See App C.2

4.3 Learning an Expert-Agnostic Deferral Mechanism

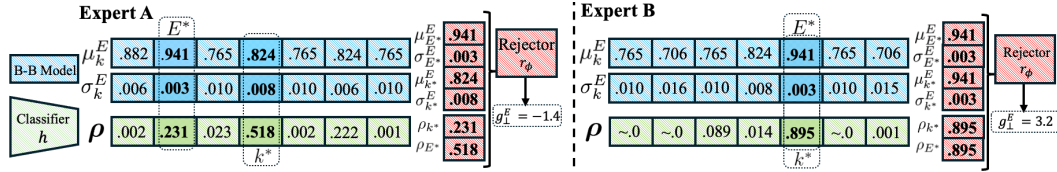


Figure 2: Example rejector inputs/outputs. Expert A: Classifier uncertain, expert highly competent \Rightarrow negative g_\perp (no deferral). Expert B: Classifier confident and prediction aligns with expert’s expertise \Rightarrow positive g_\perp (deferral).

Having constructed the expert’s probabilistic behavioural representation $\mathcal{R}^E = [(\mu_k^E, (\sigma_k^E)^2)]_{k=1}^K$, the system must decide whether to defer based on a comparison between the classifier’s prediction and the expert’s estimated competence. We instantiate this decision process using a learned rejector network, r_ϕ , whose operational logic is designed to be *expert-agnostic*.

To make a principled deferral judgement for a given input \mathbf{x}^Q , r_ϕ requires evidence comparing the classifier’s confidence against the expert’s reliability at the most salient classes: the classifier’s own most probable prediction, $k^* = \arg \max_k \rho_k$ (where ρ is the classifier’s softmax output), and the expert’s identified primary expertise class, $E^* = \arg \max_k \mu_k^E$. The network receives a state vector comprising: (a) the classifier’s peak confidence ρ_{k^*} ; (b) the expert’s estimated performance $(\mu_{k^*}^E, (\sigma_{k^*}^E)^2)$ at the classifier’s predicted class k^* ; (c) the expert’s peak estimated performance $(\mu_{E^*}^E, (\sigma_{E^*}^E)^2)$ at their primary expertise class E^* ; and (d) the classifier’s confidence ρ_{E^*} at the expert’s strongest class E^* . The rejector network r_ϕ then maps this state vector to the deferral logit:

$$g_\perp^E = r_\phi \left(\underbrace{\rho_{k^*}, \rho_{E^*}}_{\text{Classifier Signals}}, \underbrace{\mu_{k^*}^E, (\sigma_{k^*}^E)^2}_{\text{Expert @ Pred } k^*}, \underbrace{\mu_{E^*}^E, (\sigma_{E^*}^E)^2}_{\text{Expert Peak @ Best } E^*} \right)$$

Figure 2 provides illustrative examples of this mechanism. Crucially, the inputs to r_ϕ are solely numerical confidence values and statistical moments derived from \mathcal{R}^E , evaluated at the dynamically identified classes k^* and E^* . The network receives neither the absolute identities (i.e., labels) of k^* or E^* , nor any explicit identifier for the expert E . This input design enforces the *expert-agnostic* property: r_ϕ learns a deferral policy based purely on the *structural relationship* between the classifier’s certainty and the expert’s statistical performance profile, irrespective of the specific semantic classes involved.

Proposition 3. *EA-L2D’s deferral mechanism is expert-agnostic, such that for any two experts with identical performance statistics relative to their respective expertise classes, the deferral decisions are identical when facing inputs that produce structurally equivalent classifier confidence patterns, regardless of the specific class labels involved. Proof: See App. A.2.2.*

This statistical invariance, formally stated in Prop. 3, is paramount for the robust generalisation to out-of-distribution experts whose specialisations might involve classes entirely unseen during training, as the learned logic remains structurally applicable.

4.4 Optimisation Incorporating Uncertainty with Reduced Annotations

To train EA-L2D without requiring expert annotations m on the query set \mathcal{D}_Q , we adapt the standard surrogate loss \mathcal{L}_{CE} (Eq. (2)). The core modification involves replacing the ground-truth deferral

condition $\mathbb{I}[m = y^Q]$ with an evidence-based approximation derived from the expert representation \mathcal{R}^E . Specifically, we approximate the condition $m = y^Q$ using $\mathbb{I}[E^* = y^Q]$ (where E^* is the expert’s estimated primary expertise class) indicating the query likely falls within the expert’s area of strength. Furthermore, to incorporate the uncertainty inherent in estimating expert performance from limited context data, we weight this condition using a risk-sensitive Lower Confidence Bound (LCB):

$$w_{y^Q}^E := \max(0, \mu_{k=y^Q}^E - \alpha \sigma_{k=y^Q}^E), \quad (3)$$

where $\mu_{k=y^Q}^E$ and $\sigma_{k=y^Q}^E$ are the posterior mean and standard deviation of the expert’s accuracy for the true query class y^Q (obtained from \mathcal{R}^E), and $\alpha \geq 0$ (default $\alpha = 1$) controls the pessimism. This LCB weight tempers the deferral incentive when accuracy estimates are uncertain (i.e., high $\sigma_{k=y^Q}^E$), particularly useful when context data is sparse. Combining these yields the EA-L2D surrogate loss:

$$\mathcal{L}_{EA-LCE}(g; \mathbf{x}^Q, y^Q, \mathcal{R}_E) = -\log P(y^Q | \mathbf{x}^Q; g) - w_{y^Q}^E \mathbb{I}[E^* = y^Q] \log P(\perp | \mathbf{x}^Q, \mathcal{R}_E; g), \quad (4)$$

where $P(y' | \cdot; g)$ is the softmax over g . Our EA-LCE surrogate loss adapts the Bayes-consistent LCE framework [22]. Theoretical analysis (App C.3) establishes that its LCB weight converges to the true expert accuracy (Prop. C.1). Furthermore, in the infinite-context limit, minimising the EA-LCE loss yields the Bayes-optimal classifier and induces a specific, interpretable deferral rule that strategically leverages the expert’s competence in their identified area of strength (Thm. C.3). An ablation study showed that uncertainty-aware LCB weighting in EA-L2D improves robustness to uncertain, low-skill experts over uncertainty-agnostic variants, without sacrificing overall performance (see App F.4)

5 Experiments

We conduct experiments to validate EA-L2D. Our primary research questions (RQs) are:

- **RQ1:** *How does EA-L2D compare to state-of-the-art methods, particularly in terms of robustness to unseen experts and varying expert diversity?*
- **RQ2:** *How does performance scale with experts possessing multiple areas of expertise?*
- **RQ3:** *What is the effect of incorporating prior knowledge, especially under limited context data?*

Additional RQs, including **RQ4:** *How does performance scale with increasing context data for EA-L2D versus baselines?*, and **RQ5:** *How robust is EA-L2D compared to L2D-Pop under input distribution shift?* are provided in App F. To address these RQs, we first detail datasets, evaluation metrics, expert simulation, and baselines, followed by the experimental findings for each RQ. We conclude by qualitatively examining *why* EA-L2D outperforms L2D-Pop in OOD generalisation. See App. D for implementation details.

Datasets We utilise four medical datasets: **HAM10000** [23] (dermatological), **Blood Cells** [24] (microscopic), **Retinal OCT** [25] (OCT), and **Liver Tumours** [26] (radiological). These cover standard benchmarks and realistic, high-stakes medical scenarios over varying modalities.

Evaluation Metrics for Variable Deferral Budgets Evaluating L2D systems at their default operational point ($g_{\perp} \geq \max_k g_k(\mathbf{x})$) overlooks performance trade-offs across different *deferral budgets* (fractions of cases deferred). To assess performance comprehensively, we adapt the Area Under the Accuracy-Rejection Curve (AUARC) [27]. Cases are ranked for deferral using the priority score $\perp_i^E := g_{\perp}^E - \max_k g_k(\mathbf{x}_i^Q)$. Thresholding this score simulates deferring any fraction $d \in [0, 1]$ of cases. We measure performance across this range using two integrated metrics:

- **Area Under the Rejection System Accuracy Curve (AURSAC):** Average overall system accuracy (‘SysAcc(d)’, combining classifier and expert performance) across all deferral fractions d .
- **Area Under the Rejection Deferral Accuracy Curve (AURDAC):** Average expert accuracy specifically on deferred cases (‘ExpAcc(d)’) across all deferral fractions d .

These metrics assess the overall expert-AI collaboration quality (AURSAC) and the effectiveness of deferring to competent experts (AURDAC). They can be computed over desired specific intervals $[d_{\min}, d_{\max}]$ for analysing performance within particular operational regimes (e.g., “risk-tolerant, low deferral capacity”: $d \in [0, 0.1]$, or “risk-averse, high deferral capacity”: $d \in [0, 0.5]$):

$$\text{AURSAC}(d_{\min}, d_{\max}) := \frac{\int_{d_{\min}}^{d_{\max}} \text{SysAcc}(d) dd}{d_{\max} - d_{\min}}, \quad \text{AURDAC}(d_{\min}, d_{\max}) := \frac{\int_{d_{\min}}^{d_{\max}} \text{ExpAcc}(d) dd}{d_{\max} - d_{\min}},$$

where integrals are approximated numerically. Normalisation by $(d_{\max} - d_{\min})$ enables comparison of average performance across varying dataset sizes.

Simulated Experts We follow the established simulation protocol of Tailor et al. [2]. This approach is necessitated by the current unavailability of suitable real-world multi-expert datasets in sensitive domains (due to privacy and logistical constraints). Crucially, it allows for controlled evaluation of performance across varying expertise levels and the critical assessment of generalisation to experts with previously unseen specialisations, aligning with our goal of evaluating expert-agnostic robustness. Each expert has a unique expertise class (oracle accuracy), predicting correctly on others with overlap probability p and uniformly at random otherwise. We vary $p \in \{0.2, 0.5, 0.8\}$ (low p : specialised, high p : overlapping skills) and split classes into in-distribution (ID) and out-of-distribution (OOD). At inference, the system defers samples i to the expert with the highest deferral priority \perp_i^E .

Baselines We evaluate EA-L2D relative to three baselines:

- **L2D-Pop** [2]: The current SOTA for L2D adapting to unseen experts via meta-learning.
- **Pop-Avg**: A natural baseline adapting standard L2D [22] to the population setting by using the mode expert prediction on query data to drive the deferral loss. Full formulation in Appendix E.
- **Multi-Expert L2D** [5]: The standard baseline for deferring to a fixed set of experts. Evaluated only on ID experts, as it cannot handle flexible experts by design.

5.1 RQ1: Performance Comparison Across Expert Diversity

Table 1: Performance comparison of EA-L2D, L2D-Pop, Pop-Avg, and Multi-Expert L2D on the **HAM10000**, **Blood Cells**, **Retinal OCT**, and **Liver Tumour** datasets over $p \in \{0.2, 0.5, 0.8\}$, using both in-distribution (ID) and out-of-distribution (OOD) experts. Results are reported as mean \pm std.dev. across 10 randomly sampled expert cohorts. **Bold** indicates the statistically significant best result (two-tailed paired t -test, $\alpha = 0.05$) for both SAC and DAC (AURSAC(0,1) and AURDAC(0,1), respectively). The Δ SAC column reports the SAC difference between EA-L2D and the next best method. \dagger indicates a statistically significant difference between ID and OOD results (two-tailed paired t -test, $\alpha = 0.05$).

Dataset	p	Experts		EA-L2D (Ours)		L2D-Pop (Tailor et al. [2])		Pop-Avg (Natural Baseline)		Multi-Exp. L2D (Verma et al. [5])	
			Δ SAC	SAC \uparrow	DAC \uparrow	SAC \uparrow	DAC \uparrow	SAC \uparrow	DAC \uparrow	SAC \uparrow	DAC \uparrow
HAM10000 [23] $K = 7$ Classes 3/4 ID/OOD Experts $N_G^E = 105$ Cntx Preds Dermatological Img.	.2	ID	+02	.76\pm.08	.65\pm.15	.74 \pm .08	.61 \pm .16	.65 \pm .03	.42 \pm .05	.64 \pm .03	.42 \pm .07
		OOD	+10	.75\pm.08	.60\pm.05\dagger	.65 \pm .08 \dagger	.43 \pm .11 \dagger	.65 \pm .03	.40 \pm .05 \dagger	N/A	N/A
	.5	ID	+03	.83\pm.05	.77\pm.09	.80 \pm .05	.70 \pm .09	.77 \pm .02	.64 \pm .04	.76 \pm .01	.63 \pm .03
		OOD	+07	.83\pm.05	.78\pm.10	.75 \pm .05 \dagger	.63 \pm .07 \dagger	.76 \pm .02	.63 \pm .04	N/A	N/A
	.8	ID	.00	.89\pm.03	.90\pm.04	.89\pm.02	.88\pm.04	.88 \pm .01	.85 \pm .02	.87 \pm .01	.85 \pm .02
		OOD	+03	.89\pm.03	.90\pm.04	.86 \pm .01 \dagger	.84 \pm .02 \dagger	.88 \pm .01	.85 \pm .02	N/A	N/A
Blood Cells [24] $K = 8$ Classes 4/4 ID/OOD Experts $N_G^E = 120$ Cntx Preds Microscopic Img.	.2	ID	.00	.82\pm.04	.76\pm.08	.82\pm.03	.70 \pm .04	.67 \pm .01	.38 \pm .02	.66 \pm .01	.39 \pm .01
		OOD	+18	.83\pm.03	.78\pm.04	.65 \pm .02 \dagger	.34 \pm .03 \dagger	.65 \pm .01	.34 \pm .01 \dagger	N/A	N/A
	.5	ID	+01	.87\pm.03	.83\pm.07	.86\pm.02	.77 \pm .04	.78 \pm .01	.60 \pm .02	.77 \pm .01	.60 \pm .01
		OOD	+09	.87\pm.03	.84\pm.05	.78 \pm .01 \dagger	.60 \pm .02 \dagger	.78 \pm .01	.59 \pm .01 \dagger	N/A	N/A
	.8	ID	.00	.93\pm.01	.93\pm.02	.93\pm.01	.89 \pm .02	.90 \pm .01	.84 \pm .01	.90 \pm .01	.84 \pm .01
		OOD	+03	.93\pm.02	.93\pm.03	.90 \pm .00 \dagger	.84 \pm .01 \dagger	.90 \pm .01	.84 \pm .01	N/A	N/A
Retinal OCT [25] $K = 4$ 2/2 ID/OOD Experts $N_G^E = 60$ Cntx Preds OCT Img.	.2	ID	-.01	.69\pm.02	.71\pm.05	.70\pm.01	.69 \pm .05	.65 \pm .01	.59 \pm .03	.60 \pm .10	.58 \pm .04
		OOD	+07	.69\pm.02	.71\pm.07	.62 \pm .03 \dagger	.53 \pm .06 \dagger	.62 \pm .02 \dagger	.53 \pm .03 \dagger	N/A	N/A
	.5	ID	+00	.75\pm.01	.83\pm.03	.75\pm.02	.80 \pm .03	.73 \pm .01	.74 \pm .02	.70 \pm .07	.73 \pm .03
		OOD	+05	.75\pm.02	.81\pm.04	.70 \pm .02 \dagger	.71 \pm .04 \dagger	.72 \pm .01	.71 \pm .02 \dagger	N/A	N/A
	.8	ID	+00	.81\pm.01	.92\pm.02	.81\pm.01	.91 \pm .02	.81\pm.01	.89 \pm .02	.81\pm.01	.89 \pm .01
		OOD	+00	.80\pm.01	.92\pm.02	.80\pm.01\dagger	.88 \pm .02 \dagger	.80\pm.01	.88 \pm .02 \dagger	N/A	N/A
Liver Tumours [26] $K = 11$ 5/6 ID/OOD Experts $N_G^E = 165$ Cntx Preds Radiological Img.	.2	ID	+01	.85\pm.02	.81\pm.04	.84 \pm .02	.72 \pm .03	.66 \pm .01	.36 \pm .03	.67 \pm .02	.36 \pm .04
		OOD	+16	.82\pm.03\dagger	.75\pm.05\dagger	.66 \pm .01 \dagger	.34 \pm .03 \dagger	.65 \pm .01	.32 \pm .02 \dagger	N/A	N/A
	.5	ID	+07	.89\pm.01	.87\pm.02	.82 \pm .03	.66 \pm .06	.78 \pm .01	.59 \pm .03	.78 \pm .01	.59 \pm .02
		OOD	+12	.90\pm.01	.88\pm.02	.78 \pm .01 \dagger	.58 \pm .03 \dagger	.78 \pm .01	.59 \pm .02	N/A	N/A
	.8	ID	+02	.93\pm.01	.93\pm.03	.91 \pm .01	.84 \pm .02	.91 \pm .01	.83 \pm .02	.91 \pm .01	.83 \pm .02
		OOD	+03	.94\pm.01	.93\pm.02	.91 \pm .01 \dagger	.83 \pm .01 \dagger	.91 \pm .01	.82 \pm .03	N/A	N/A

We evaluated EA-L2D and baselines across all datasets, varying the overlap probability p . Table 1 reports the AURSAC(0,1) and AURDAC(0,1) results for both ID and OOD experts. For direct comparison of ID-to-OOD performance differential, OOD results show performance on ID experts after training models using only OOD experts. **Findings:** EA-L2D outperforms baselines in both deferral (AURDAC) and system (AURSAC) performance, especially for OOD experts under high diversity (low p). Notably, it achieves this using a default uninformative prior (i.e. no prior knowledge regarding expert’s expertise). Practically, this performance gain comes with significant annotation

savings; EA-L2D avoids the $E \times N_Q$ query set annotations required by L2D-Pop, needing only context set labels ($\sum_E N_C^E$). Since query sets are typically much larger than context sets (e.g., **Blood Cells**: $N_Q = 11959$, $N_C^E = 120$), EA-L2D considerably reduces the annotation burden. These results provide empirical support to our proposed LCB-weighted expert proxy loss (Eq. 4). Furthermore, EA-L2D’s expert-agnosticism is empirically supported by its OOD robustness: L2D-Pop always shows a statistically significant ID-to-OOD performance decrease (indicated by \dagger), while EA-L2D rarely experiences such performance degradation across expert distribution shifts.

5.2 RQ2: Multi-Expertise Experts

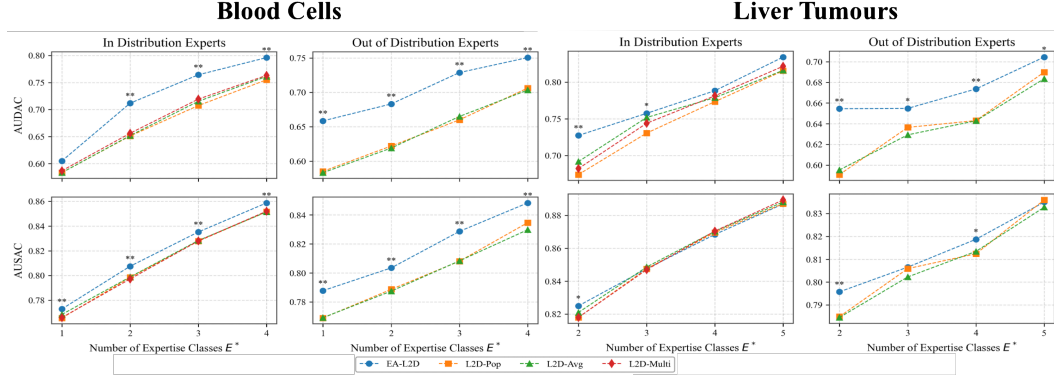


Figure 3: Performance comparison between EA-L2D and L2D-Pop using a single in-distribution (ID) and out-of-distribution (OOD) expert, across varying numbers of expertise classes (E^*), on **Liver Tumours** and **Blood Cells** datasets. Asterisks denote statistical significance in favour of EA-L2D: * for $p < 0.1$ and ** for $p < 0.05$ (via two-tailed paired samples t-test).

To address RQ2, we simulated one ID and one OOD expert with $p = 0.5$ for both **Liver Tumours** and **Blood Cells**, varying the number of expertise classes E^* . For each setting, we randomly generated 10 cohorts of ID/OOD experts by sampling their expertise classes at random. Training was conducted on ID experts, with evaluation performed on both ID and OOD experts. Figure 3 shows the AURSAC comparison between EA-L2D and baselines. **Findings:** EA-L2D maintains performance superiority when experts possess multiple areas of specialisation. On both datasets, EA-L2D shows superior performance for both ID and OOD experts as the number of expertise classes increases, with a more pronounced effect on OOD evaluation. These results indicate that EA-L2D’s ability to maintain and access distinct per-class performance metrics in its behavioural representation is key to effectively leveraging an expert’s multiple specialisations.

5.3 RQ3: Impact of Prior Knowledge and Context Data Interaction

To investigate how prior knowledge interacts with available context data, we simulated a scenario with HAM10000. We defined a simulated expert with true expertise in class 3 (Benign Keratosis-like lesions), with $\bar{\theta}_3^{(E)} = 0.95$ and $\bar{\theta}_{k \neq 3}^{(E)} = 0.4$. We then evaluated EA-L2D under varying amounts of context data and different prior specifications for the expert, keeping prior strength $s = 15$. Alternative expert simulations are provided in App F.1. We then evaluated the following priors: (1) **Accurate Informative Prior:** Assumes accurate self-assessment ($p_3 = 0.95$, $c_3 = 0.9$), (2) **Uninformative Prior:** Default Beta(1, 1), and (3) **Inaccurate (Misspecified) Prior:** Incorrectly specified expertise in class 0 ($p_0 = 0.95$, $c_0 = 0.9$). **Findings:** Fig. 4 presents the resulting AURSAC scores. The results demonstrate that accurate priors significantly boost performance equivalent to ≈ 50 context points. As context data increases, the detrimental impact of the incorrect informative prior diminishes rapidly, empirically supporting Prop. 2 that sufficient data overcomes initial prior specification.

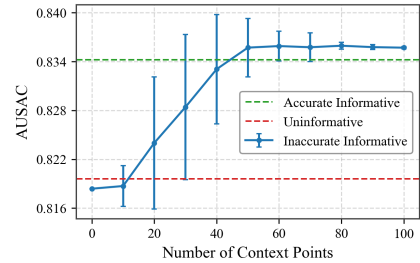


Figure 4: Effect of prior knowledge on EA-L2D performance (AURSAC) for a Class 3 HAM10000 expert.

5.4 Characterising L2D-Pop’s Latent Space and its Implications for OOD Generalisation

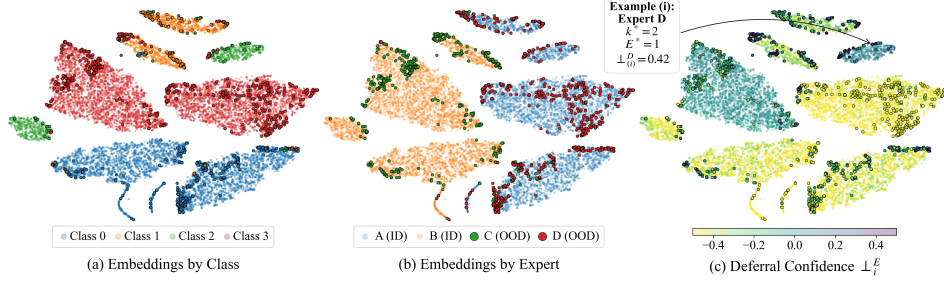


Figure 5: Latent behavioural representations learned by L2D-Pop on **Retinal OCT**, visualised by (a) predicted class, (b) expert identity, and (c) deferral confidence. Outlined circles indicate OOD experts with test images; faded, non-outlined faded circles represent training images from ID experts.

To qualitatively assess L2D-Pop’s OOD degradation (RQ1), we examine its latent behavioural representations on the **Retinal OCT** dataset ($p = 0.2$, $K = 4$; Fig. 5) by projecting the high-dimensional representations to 2D using t-SNE. For ID Experts A (expertise class 3) and B (expertise class 2), L2D-Pop forms clear class-expertise clusters, correctly deferring within these (Fig. 5a–c, blue clusters in c). When we embed test-time OOD Experts C and D’s representations onto the learned projection (via `openTSNE` [28, 29], outlined dots in Fig. 5b), however, we see these project onto ID manifolds, not novel class-expertise clusters. E.g., for Expert D (Example (i)), the classifier predicts Class 2 (Expert B’s domain). Despite deferral being inappropriate here, L2D-Pop assigns high priority ($\perp^D = 0.42$) vs EA-L2D’s low value ($\perp^D = -0.95$). We hypothesise L2D-Pop overfits ID expert specialisations, entangling embeddings and misrepresenting OOD experts via projection onto nearest ID manifolds (C, D in Fig. 5b). This leads to erroneous deferrals (Example (i)), as Expert D inherits priority due to resemblance to ID Expert B. Reliance on holistic training-based profiles hampers OOD generalisation, a pitfall EA-L2D avoids via explicit, class-wise statistical representations that enable more robust adaptation to unseen experts.

6 Conclusion and Limitations

We introduced Expert-Agnostic Learning to Defer (EA-L2D), addressing adaptability and data efficiency limits in L2D systems. By constructing explicit, interpretable expert representations via a Bayesian approach, EA-L2D achieves inherent expert-agnosticism. This design offers substantial advantages over the previous state-of-the-art (see Tab. 2). Experiments confirm EA-L2D’s superior system-wise and deferral performance, especially against unseen experts.

Table 2: Key comparison between EA-L2D and L2D-Pop.

Aspect	EA-L2D (Ours)	L2D-Pop
Representation Type	Constructed (Explicit)	Learned (Latent)
OOD Generalisation	Expert-Agnostic	Overfits to ID Experts
Prior Knowledge	Supported (✓)	Not Supported (×)
Annotation Needs	Context Only	Context + Query
Interpretability	High (Via Metrics)	Low (Latent Vector)
Optimisation Method	Standard Supervised	Meta-learning
Computational Efficiency	Higher (see §A.3)	Lower (see §A.3)

Limitations Whilst the option to incorporate prior knowledge into EA-L2D can be valuable, inaccurate priors may have a detrimental effect, particularly when context data is sparse. This concern is lessened by two factors: our method performs strongly using default uninformative priors (Tab. 1), and secondly, both empirical evidence (Fig. 4, App F.1) and theory (Prop. 2) show that sufficient context data can overcome the influence of an inaccurate prior. Another consideration is our expert representation, \mathcal{R}^E . Its explicit, class-wise summary of statistics is central to its interpretability and the strong OOD expert performance we observe (Section 5.4). However, this structured approach might provide a more generalised, and thus potentially coarser, view of an expert’s behaviour compared to very detailed latent embeddings. If future techniques can improve upon the work of L2D-Pop and learn fine-grained high-dimensional latent representations from limited data (whilst alleviating the issues we have highlighted in this paper) they could offer a path to further improvements in performance.

References

- [1] David Madras, Toniann Pitassi, and Richard Zemel. Predict responsibly: Improving fairness and accuracy by learning to defer, 2018. URL <https://arxiv.org/abs/1711.06664>.
- [2] Dharmesh Tailor, Aditya Patra, Rajeev Verma, Putra Manggala, and Eric Nalisnick. Learning to defer to a population: A meta-learning approach, 2024. URL <https://arxiv.org/abs/2403.02683>.
- [3] C. K. Chow. An optimum character recognition system using decision functions. *IRE Transactions on Electronic Computers*, EC-6(4):247–254, 1957. doi: 10.1109/TEC.1957.5222035.
- [4] C. Chow. On optimum recognition error and reject tradeoff. *IEEE Transactions on Information Theory*, 16(1):41–46, 1970. doi: 10.1109/TIT.1970.1054406.
- [5] Rajeev Verma, Daniel Barrejón, and Eric Nalisnick. Learning to defer to multiple experts: Consistent surrogate losses, confidence calibration, and conformal ensembles, 2023. URL <https://arxiv.org/abs/2210.16955>.
- [6] Anqi Mao, Mehryar Mohri, and Yutao Zhong. Principled approaches for learning to defer with multiple experts, 2024. URL <https://arxiv.org/abs/2310.14774>.
- [7] Patrick Hemmer, Lukas Thede, Michael Vössing, Johannes Jakubik, and Niklas Kühl. Learning to defer with limited expert predictions, 2023. URL <https://arxiv.org/abs/2304.07306>.
- [8] Anonymous. Probabilistic learning to defer: Handling missing expert annotations and controlling workload distribution. In *Submitted to The Thirteenth International Conference on Learning Representations*, 2024. URL <https://openreview.net/forum?id=z10HLZOJC9>. under review.
- [9] Jean V. Alves, Diogo Leitão, Sérgio Jesus, Marco O. P. Sampaio, Javier Liébana, Pedro Saleiro, Mário A. T. Figueiredo, and Pedro Bizarro. Cost-sensitive learning to defer to multiple experts with workload constraints, 2024. URL <https://arxiv.org/abs/2403.06906>.
- [10] Zheng Zhang, Wenjie Ai, Kevin Wells, David Rosewarne, Thanh-Toan Do, and Gustavo Carneiro. Learning to complement and to defer to multiple users. In *European Conference on Computer Vision*, pages 144–162. Springer, 2025.
- [11] Anqi Mao, Christopher Mohri, Mehryar Mohri, and Yutao Zhong. Two-stage learning to defer with multiple experts. In *Thirty-seventh Conference on Neural Information Processing Systems*, 2023. URL <https://openreview.net/forum?id=GIIsH0T4b2>.
- [12] Yannis Montreuil, Axel Carlier, Lai Xing Ng, and Wei Tsang Ooi. Why ask one when you can ask k ? two-stage learning-to-defer to a set of experts, 2025. URL <https://arxiv.org/abs/2504.12988>.
- [13] Shalmali Joshi, Sonali Parbhoo, and Finale Doshi-Velez. Learning-to-defer for sequential medical decision-making under uncertainty. *arXiv preprint arXiv:2109.06312*, 2021.
- [14] Joshua Strong, Qianhui Men, and J Alison Noble. Trustworthy and practical AI for healthcare: A guided deferral system with large language models. *Proc. Conf. AAAI Artif. Intell.*, 39(27): 28413–28421, April 2025.
- [15] Jean V Alves, Diogo Leitão, Sérgio Jesus, Marco OP Sampaio, Pedro Saleiro, Mário AT Figueiredo, and Pedro Bizarro. Fifar: A fraud detection dataset for learning to defer. *arXiv preprint arXiv:2312.13218*, 2023.
- [16] Thodoris Lykouris and Wentao Weng. Learning to defer in content moderation: The human-ai interplay, 2024. URL <https://arxiv.org/abs/2402.12237>.
- [17] Hyunjik Kim, Andriy Mnih, Jonathan Schwarz, Marta Garnelo, Ali Eslami, Dan Rosenbaum, Oriol Vinyals, and Yee Whye Teh. Attentive neural processes. In *International Conference on Learning Representations*, 2019. URL <https://openreview.net/forum?id=SkE6PjC9KX>.

- [18] Minyoung Kim and Timothy Hospedales. A hierarchical bayesian model for few-shot meta learning. In *The Twelfth International Conference on Learning Representations*, 2024. URL <https://openreview.net/forum?id=mQ72XRfYRZ>.
- [19] Chelsea Finn, Pieter Abbeel, and Sergey Levine. Model-agnostic meta-learning for fast adaptation of deep networks, 2017. URL <https://arxiv.org/abs/1703.03400>.
- [20] Muhammad Abdullah Jamal, Guo-Jun Qi, and Mubarak Shah. Task-agnostic meta-learning for few-shot learning, 2018. URL <https://arxiv.org/abs/1805.07722>.
- [21] Mehryar Mohri, Gary Sivek, and Ananda Theertha Suresh. Agnostic federated learning, 2019. URL <https://arxiv.org/abs/1902.00146>.
- [22] Hussein Mozannar and David Sontag. Consistent estimators for learning to defer to an expert, 2021. URL <https://arxiv.org/abs/2006.01862>.
- [23] Philipp Tschandl, Cliff Rosendahl, and Harald Kittler. The ham10000 dataset, a large collection of multi-source dermatoscopic images of common pigmented skin lesions. *Scientific Data*, 5(1), August 2018. ISSN 2052-4463. doi: 10.1038/sdata.2018.161. URL <http://dx.doi.org/10.1038/sdata.2018.161>.
- [24] Andrea Acevedo, Anna Merino, Santiago Alf  rez,   ngel Molina, Laura Bold  , and Jos   Rodellar. A dataset of microscopic peripheral blood cell images for development of automatic recognition systems. *Data in Brief*, 30:105474, 2020. ISSN 2352-3409. doi: <https://doi.org/10.1016/j.dib.2020.105474>. URL <https://www.sciencedirect.com/science/article/pii/S2352340920303681>.
- [25] Daniel S. Kermany, Michael Goldbaum, Wenjia Cai, Carolina C.S. Valentim, Huiying Liang, Sally L. Baxter, Alex McKeown, Ge Yang, Xiaokang Wu, Fangbing Yan, Justin Dong, Made K. Prasadha, Jacqueline Pei, Magdalene Y.L. Ting, Jie Zhu, Christina Li, Sierra Hewett, Jason Dong, Ian Ziyar, Alexander Shi, Runze Zhang, Lianghong Zheng, Rui Hou, William Shi, Xin Fu, Yaou Duan, Viet A.N. Huu, Cindy Wen, Edward D. Zhang, Charlotte L. Zhang, Oulan Li, Xiaobo Wang, Michael A. Singer, Xiaodong Sun, Jie Xu, Ali Tafreshi, M. Anthony Lewis, Huimin Xia, and Kang Zhang. Identifying medical diagnoses and treatable diseases by image-based deep learning. *Cell*, 172(5):1122–1131.e9, 2018. ISSN 0092-8674. doi: <https://doi.org/10.1016/j.cell.2018.02.010>. URL <https://www.sciencedirect.com/science/article/pii/S0092867418301545>.
- [26] Patrick Bilic, Patrick Christ, Hongwei Bran Li, Eugene Vorontsov, Avi Ben-Cohen, Georgios Kaissis, Adi Szeskin, Colin Jacobs, Gabriel Efrain Humpire Mamani, Gabriel Chartrand, Fabian Loh  fer, Julian Walter Holch, Wieland Sommer, Felix Hofmann, Alexandre Hostettler, Naama Lev-Cohain, Michal Drozdal, Michal Marianne Amitai, Refael Vivanti, Jacob Sosna, Ivan Ezhov, Anjany Sekuboyina, Fernando Navarro, Florian Kofler, Johannes C. Paetzold, Suprosanna Shit, Xiaobin Hu, Jana Lipkov  , Markus Rempfler, Marie Piraud, Jan Kirschke, Benedikt Wiestler, Zhiheng Zhang, Christian H  lsemeyer, Marcel Beetz, Florian Ettlinger, Michela Antonelli, Woong Bae, M  riam Bellver, Lei Bi, Hao Chen, Grzegorz Chlebus, Erik B. Dam, Qi Dou, Chi-Wing Fu, Bogdan Georgescu, Xavier Gir   i Nieto, Felix Gruen, Xu Han, Pheng-Ann Heng, J  rgen Hesser, Jan Hendrik Moltz, Christian Igel, Fabian Isensee, Paul J  ger, Fucang Jia, Krishna Chaitanya Kaluva, Mahendra Khened, Ildoo Kim, Jae-Hun Kim, Sungwoong Kim, Simon Kohl, Tomasz Konopczynski, Avinash Kori, Ganapathy Krishnamurthi, Fan Li, Hongchao Li, Junbo Li, Xiaomeng Li, John Lowengrub, Jun Ma, Klaus Maier-Hein, Kevis-Kokitsi Maninis, Hans Meine, Dorit Merhof, Akshay Pai, Mathias Perslev, Jens Petersen, Jordi Pont-Tuset, Jin Qi, Xiaojuan Qi, Oliver Rippel, Karsten Roth, Ignacio Sarasua, Andrea Schenk, Zengming Shen, Jordi Torres, Christian Wachinger, Chunliang Wang, Leon Weninger, Jianrong Wu, Daguang Xu, Xiaoping Yang, Simon Chun-Ho Yu, Yading Yuan, Miao Yue, Liping Zhang, Jorge Cardoso, Spyridon Bakas, Rickmer Braren, Volker Heinemann, Christopher Pal, An Tang, Samuel Kadoury, Luc Soler, Bram van Ginneken, Hayit Greenspan, Leo Joskowicz, and Bjoern Menze. The liver tumor segmentation benchmark (lits). *Medical Image Analysis*, 84:102680, 2023. ISSN 1361-8415. doi: <https://doi.org/10.1016/j.media.2022.102680>. URL <https://www.sciencedirect.com/science/article/pii/S1361841522003085>.

- [27] Malik Sajjad Ahmed Nadeem, Jean-Daniel Zucker, and Blaise Hanczar. Accuracy-rejection curves (arcs) for comparing classification methods with a reject option. In Sašo Džeroski, Pierre Guerts, and Juho Rousu, editors, *Proceedings of the third International Workshop on Machine Learning in Systems Biology*, volume 8 of *Proceedings of Machine Learning Research*, pages 65–81, Ljubljana, Slovenia, 05–06 Sep 2009. PMLR. URL <https://proceedings.mlr.press/v8/nadeem10a.html>.
- [28] Pavlin G. Poličar, Martin Stražar, and Blaž Zupan. opentsne: A modular python library for t-sne dimensionality reduction and embedding. *Journal of Statistical Software*, 109(3):1–30, 2024. doi: 10.18637/jss.v109.i03. URL <https://www.jstatsoft.org/index.php/jss/article/view/v109i03>.
- [29] Pavlin G. Poličar, Martin Stražar, and Blaž Zupan. Embedding to reference t-sne space addresses batch effects in single-cell classification. *Machine Learning*, 112(2):721–740, August 2021. ISSN 1573-0565. doi: 10.1007/s10994-021-06043-1. URL <http://dx.doi.org/10.1007/s10994-021-06043-1>.
- [30] Hyunjik Kim, Andriy Mnih, Jonathan Schwarz, Marta Garnelo, Ali Eslami, Dan Rosenbaum, Oriol Vinyals, and Yee Whye Teh. Attentive neural processes, 2019. URL <https://arxiv.org/abs/1901.05761>.
- [31] Kaiming He, Xiangyu Zhang, Shaoqing Ren, and Jian Sun. Deep residual learning for image recognition, 2015. URL <https://arxiv.org/abs/1512.03385>.
- [32] Mingxing Tan and Quoc V. Le. Efficientnet: Rethinking model scaling for convolutional neural networks, 2020. URL <https://arxiv.org/abs/1905.11946>.
- [33] Mark Sandler, Andrew Howard, Menglong Zhu, Andrey Zhmoginov, and Liang-Chieh Chen. Mobilenetv2: Inverted residuals and linear bottlenecks, 2019. URL <https://arxiv.org/abs/1801.04381>.
- [34] Diederik P. Kingma and Jimmy Ba. Adam: A method for stochastic optimization, 2017. URL <https://arxiv.org/abs/1412.6980>.
- [35] Carlos Hernández-Pérez, Marc Combalia, Sebastian Podlipnik, Noel C. F. Codella, Veronica Rotemberg, Allan C. Halpern, Ofer Reiter, Cristina Carrera, Alicia Barreiro, Brian Helba, Susana Puig, Veronica Vilaplana, and Josep Malvehy. Bcn20000: Dermoscopic lesions in the wild. *Scientific Data*, 11(1), June 2024. ISSN 2052-4463. doi: 10.1038/s41597-024-03387-w. URL <http://dx.doi.org/10.1038/s41597-024-03387-w>.

A Additional Discussions

A.1 Expert Representation: Constructed Bayesian vs. Learned Latent

A fundamental distinction between EA-L2D and the L2D-Pop framework [2] lies in how they represent expert behaviour using context data \mathcal{D}_C^E . EA-L2D employs a Bayesian statistical model to directly *construct* an explicit representation based on performance metrics, whereas L2D-Pop takes a meta-learning approach, utilising an Attentive Neural Process (ANP) [17], to *learn* a latent representation.

EA-L2D: Constructed Bayesian Representation (\mathcal{R}^E) As detailed in §4.1, EA-L2D applies a conjugate Beta-Binomial model directly to the context data \mathcal{D}_C^E to estimate the posterior distribution of each class-wise accuracy θ_k^E . The resulting representation \mathcal{R}^E is a structured collection of interpretable statistical summaries: the posterior mean μ_k^E and posterior variance $(\sigma_k^E)^2$ for each class k :

$$\mathcal{R}^E = [(\mu_{k=1}^E, (\sigma_{k=1}^E)^2), \dots, (\mu_{k=K}^E, (\sigma_{k=K}^E)^2)].$$

The choice of the Beta-Binomial framework is motivated by several key advantages for modelling expert performance from potentially limited data:

- **Principled Prior Integration:** Its Bayesian nature supports incorporating prior knowledge (§4.2).

- **Explicit Uncertainty Quantification:** The posterior variance $(\sigma_k^E)^2$ directly measures epistemic uncertainty, crucial for robustness with sparse data. EA-L2D leverages this uncertainty in both the rejector input (§4.3) and the loss function’s LCB weighting (Eq. 4).
- **Interpretability:** The components $\mu_k^E, (\sigma_k^E)^2$ are transparent measures of estimated accuracy and uncertainty.
- **Efficiency & Guarantees:** Conjugacy allows efficient computation, and the model has theoretical guarantees (Prop. 1, 2).
- **Empirical Efficacy:** Experiments show this approach yields strong performance, especially for OOD experts (Tab. 1).

L2D-Pop: Learned Latent Representation (ψ^E) In contrast, L2D-Pop processes \mathcal{D}_C^E using an ANP encoder to generate point-wise representations, which are aggregated (e.g., via attention) into a single latent vector ψ^E . This vector serves as the learned, holistic representation of the expert’s behaviour. The deferral function g_\perp is then conditioned on this latent representation, i.e., $g_\perp(x, \psi^E)$, within a meta-learning framework. While powerful for capturing complex patterns, potential drawbacks include the data demands of meta-learning, potential ANP limitations [30], and crucially, the handling of uncertainty is *implicit* within the learned vector ψ^E , lacking an explicit mechanism for quantifying or utilising statistical variance like EA-L2D’s $(\sigma_k^E)^2$.

A.2 The Expert-Agnostic Deferral Mechanism of EA-L2D

Building upon its constructed representation, EA-L2D employs a deferral mechanism designed to be invariant to specific class expertise, a property we term *expert-agnostic*.

A.2.1 Motivation and Definition of Expert-Agnosticism

A core design principle of EA-L2D is its *expert-agnostic* deferral mechanism. It is crucial to precisely define what this term signifies in our context. “Expert-agnostic” does not imply that the system ignores the expert’s capabilities. Instead, it signifies that the deferral decision logic learned by the rejector network (r_ϕ) is invariant to the specific identity of the expert and the specific class labels (k^*, E^*) that happen to be relevant for a given input instance. The mechanism operates purely on the quantified, statistical relationship between the classifier’s outputs (confidence levels ρ) and the expert’s performance characteristics (posterior mean μ_k^E and variance $(\sigma_k^E)^2$ derived from the constructed representation \mathcal{R}^E).

This invariance is achieved *by design* through the specific numerical inputs provided to the rejector network r_ϕ (as detailed in §4.3). Rather than receiving expert identifiers or raw class indices, r_ϕ processes only:

1. Classifier confidences at the relevant classes (ρ_{k^*}, ρ_{E^*}).
2. Expert performance statistics (mean and variance) evaluated at these same relevant classes ($\mu_{k^*}^E, (\sigma_{k^*}^E)^2, \mu_{E^*}^E, (\sigma_{E^*}^E)^2$).

These inputs abstract the core decision problem into comparing classifier certainty against expert reliability *structurally*, detached from the specific labels involved.

The significance of this expert-agnostic property lies in its direct contribution to robust generalisation, particularly to out-of-distribution experts (those specialising in classes unseen during training). By learning deferral rules based on transferable statistical patterns (e.g., a general rule like “defer when classifier confidence ρ_{k^*} is low but the expert’s estimated accuracy $\mu_{k^*}^E$ for that predicted class is high”) rather than learning associations tied to specific class labels encountered during training (e.g., a non-transferable rule like “defer frequently if the expert’s speciality E^* is class 3”), EA-L2D’s deferral logic can be readily applied to novel experts and expertise patterns.

Conceptually, this parallels principles in other “agnostic” learning paradigms. Similar to how Model-Agnostic Meta-Learning (MAML) [19] learns a transferable initialisation process adaptable to new tasks, or Task-Agnostic Meta-Learning (TAML) [20] aims for unbiased models generalisable across tasks, EA-L2D learns a transferable *deferral evaluation function* (r_ϕ) grounded in statistical comparison, making it applicable across diverse expert profiles defined by \mathcal{R}^E , irrespective of their specific class specialisations.

The following sections formalise this property (Proposition 3 and its proof in Appendix A.2.2), detail its implications, and contrast it with alternative representation strategies.

A.2.2 Formalisation (Proof of Proposition 3)

We now formally demonstrate that EA-L2D’s deferral mechanism, relying on the specific input design for r_ϕ , satisfies the definition of expert-agnosticism. The proof establishes that if two distinct scenarios (potentially involving different experts E_1, E_2 , inputs $\mathbf{x}_1, \mathbf{x}_2$, and associated class labels $k_1^*, E_1^*, k_2^*, E_2^*$) yield the *same set of numerical input values* to r_ϕ , the resulting deferral logit g_\perp must be identical, proving invariance to the specific expert identities or class labels involved.

Proposition 3. *EA-L2D’s deferral mechanism is expert-agnostic: for any two experts with identical performance statistics relative to their respective expertise classes, the deferral decisions are identical when facing inputs that produce structurally equivalent classifier confidence patterns, regardless of the specific class labels involved.*

Proof. We demonstrate that EA-L2D’s deferral mechanism is expert-agnostic by showing that its decisions depend solely on the statistical relationship between classifier outputs and expert performance characteristics, rather than on specific class labels or expert identities. Let us consider two distinct experts E_1 and E_2 with different expertise classes $E_1^* \neq E_2^*$. For any two inputs \mathbf{x}_1 and \mathbf{x}_2 generating classifier softmax outputs ρ_1 and ρ_2 with predicted classes k_1^* and k_2^* , we examine the deferral logits $g_\perp^{E_1}(\mathbf{x}_1)$ and $g_\perp^{E_2}(\mathbf{x}_2)$.

Recall that the deferral logit is computed as:

$$g_\perp^E = r_\phi(\rho_{E^*}, \rho_{k^*}, \mu_{k^*}^E, (\sigma_{k^*}^E)^2, \mu_{E^*}^E, (\sigma_{E^*}^E)^2)$$

For experts E_1 and E_2 , we have:

$$\begin{aligned} g_\perp^{E_1} &= r_\phi(\rho_{E_1^*}^{(1)}, \rho_{k_1^*}^{(1)}, \mu_{k_1^*}^{E_1}, (\sigma_{k_1^*}^{E_1})^2, \mu_{E_1^*}^{E_1}, (\sigma_{E_1^*}^{E_1})^2) \\ g_\perp^{E_2} &= r_\phi(\rho_{E_2^*}^{(2)}, \rho_{k_2^*}^{(2)}, \mu_{k_2^*}^{E_2}, (\sigma_{k_2^*}^{E_2})^2, \mu_{E_2^*}^{E_2}, (\sigma_{E_2^*}^{E_2})^2) \end{aligned}$$

Suppose the following structural equivalence conditions hold:

$$\begin{aligned} \rho_{E_1^*}^{(1)} &= \rho_{E_2^*}^{(2)} \\ \rho_{k_1^*}^{(1)} &= \rho_{k_2^*}^{(2)} \\ \mu_{k_1^*}^{E_1} &= \mu_{k_2^*}^{E_2} \\ (\sigma_{k_1^*}^{E_1})^2 &= (\sigma_{k_2^*}^{E_2})^2 \\ \mu_{E_1^*}^{E_1} &= \mu_{E_2^*}^{E_2} \\ (\sigma_{E_1^*}^{E_1})^2 &= (\sigma_{E_2^*}^{E_2})^2 \end{aligned}$$

Since r_ϕ is a function that maps these six inputs to a scalar value, and given that all corresponding inputs are equal, it follows directly that:

$$g_\perp^{E_1}(\mathbf{x}_1) = g_\perp^{E_2}(\mathbf{x}_2)$$

This equality holds regardless of the specific identities of E_1^* and E_2^* , demonstrating that the deferral decision is invariant to permutation of class labels. The rejector makes identical decisions when the structural relationships between classifier outputs and expert capabilities are equivalent, even when the specific expertise classes differ.

To further illustrate this property, consider a permutation function $\pi : \mathcal{Y} \rightarrow \mathcal{Y}$ that maps each class to another, such that $\pi(E_1^*) = E_2^*$. If we apply this permutation to transform expert E_1 ’s representation and the classifier’s outputs for \mathbf{x}_1 , creating:

$$\begin{aligned} \hat{\rho}_j^{(1)} &= (\rho_1)_{\pi^{-1}(j)} \quad \forall j \in \mathcal{Y} \\ \hat{\mu}_j^{E_1} &= \mu_{\pi^{-1}(j)}^{E_1} \quad \forall j \in \mathcal{Y} \\ (\hat{\sigma}_j^{E_1})^2 &= (\sigma_{\pi^{-1}(j)}^{E_1})^2 \quad \forall j \in \mathcal{Y} \end{aligned}$$

Then the deferral logit computed using these transformed values would be identical to that computed for expert E_2 on input x_2 , provided the structural equivalence conditions hold.

This permutation argument explicitly illustrates that the learned function r_ϕ responds only to the *structural relationship* between classifier confidence and expert competence metrics, not to the absolute identity of the classes filling the roles of “classifier’s best guess” or “expert’s specialty”. Therefore, the learned deferral logic is inherently transferable to situations involving different specific classes.

This property is maintained regardless of the network architecture used for r_ϕ , as long as it operates on these six statistical inputs rather than on raw class identities or expert identifiers. The network learns to make deferral decisions based on the pattern of relationships between classifier confidence and expert performance, not on memorised associations between specific class labels and deferral decisions. Consequently, EA-L2D can generalise effectively to unseen experts with specialisations in previously unobserved classes, as it focuses on the statistical performance patterns rather than the specific class identities, thereby satisfying our definition of expert-agnosticism. \square

Remark A.1 (Practical Robustness of Expert-agnosticism). *The structural equivalence conditions in the proof establish a theoretical foundation for expert-agnosticism through perfect invariance. In practice, these conditions need not be exactly satisfied for the benefits of expert-agnosticism to manifest. The continuous nature of the rejector function r_ϕ ensures that similar statistical profiles lead to similar deferral decisions, with differences proportional to the degree of statistical divergence rather than specific class identities. Our empirical results confirm this property, demonstrating effective generalisation to unseen experts with novel specialisations even when perfect structural equivalence is not guaranteed. This practical robustness arises from training the rejector to focus on statistical performance patterns rather than memorising associations with specific class labels.*

A.2.3 Implications and Contrast with L2D-Pop

The expert-agnostic property of EA-L2D, arising directly from its use of a *constructed* statistical representation \mathcal{R}^E and a rejector r_ϕ operating solely on the *relationships* between classifier outputs and expert performance metrics, has significant implications for generalisation.

Specifically, this design is hypothesised to enhance robustness to out-of-distribution (OOD) experts. Because the deferral logic learned by r_ϕ is based on transferable statistical patterns (comparing confidence levels against relevant mean accuracies and variances) rather than being tied to specific class labels or expert identities seen during training, it can be more readily applied when encountering experts with novel specialisations. The system evaluates the *current situation* statistically, rather than relying on potentially learned associations from the training expert pool.

This contrasts with approaches like L2D-Pop [2], which employ mechanisms based on learned latent representations, e.g., $\psi_E = \text{ANP}(\mathcal{D}_{C_E})$, and condition the deferral decision on this embedding, $g_\perp(x, \psi_E)$. While such methods can capture complex patterns, the learned latent vector ψ^E lacks the explicit, interpretable separation of class-specific statistics found in \mathcal{R}^E . More critically for OOD generalisation, ψ^E might implicitly encode biases towards the specific types of expert behaviours encountered during meta-training. It could inadvertently learn associations with specific class identities present in the training data, rather than purely abstract statistical relationships. Consequently, its effectiveness may be limited when adapting to experts whose performance profiles differ significantly from those seen during meta-training, potentially failing to satisfy the invariance property central to our definition of expert-agnosticism.

In summary, EA-L2D’s advantage stems from its reliance on an explicitly constructed, interpretable statistical profile (\mathcal{R}^E) coupled with a deferral mechanism (r_ϕ) designed to be invariant to specific class identities. This approach aims to avoid the potential pitfalls of learned latent representations regarding OOD expert generalisation, offering a deferral logic that is inherently more transferable *by design*.

A.3 Computational Efficiency of EA-L2D Relative to L2D-Pop

EA-L2D presents notable computational advantages when compared to meta-learning approaches such as L2D-Pop. These efficiencies primarily arise from fundamental differences in how expert context data is processed to inform deferral decisions.

In EA-L2D, the expert behavioural representation, \mathcal{R}^E , is derived using a direct statistical approach based on the Beta-Binomial model (as detailed in §4.1). This calculation is efficient, scaling linearly with the number of context samples, n_C , available for an expert (specifically, $O(n_C + K)$ where K is the number of classes). This representation is constructed once per expert for a given training batch, or potentially pre-computed for known experts at inference time. The resultant static representation is then consistently applied across all relevant query samples without further re-computation related to the context data itself.

In contrast, the model-based variant of L2D-Pop, which leverages an Attentive Neural Process (ANP)-like architecture for expert context encoding, incurs a higher computational cost. To generate an expert representation, L2D-Pop processes the expert’s entire context set (of size N_C^E) for *each* individual query sample \mathbf{x}^Q (due to the cross-attention mechanism). This per-query processing involves passing context samples through embedding networks and then applying attention mechanisms (such as self-attention over context points and cross-attention between the query \mathbf{x} and the context). These attention operations can be computationally intensive, with self-attention potentially scaling quadratically with the context set size (e.g., $O(N_C^2 d_r)$, where d_r is the representation dimension).

The principal difference, therefore, lies in the per-query re-processing of the expert context set inherent in L2D-Pop’s attentive mechanism, as its expert representation is conditioned on the query \mathbf{x} . EA-L2D avoids this repeated, complex computation. This architectural distinction leads to a more computationally efficient training procedure and faster inference times for EA-L2D, particularly evident when the number of query samples is large or when context sets are of non-trivial size.

A.4 Potential Positive and Negative Societal Impacts of Our Work

The deployment of EA-L2D presents considerable potential for positive societal impact, principally by enhancing the safety and reliability of AI systems in high-stakes applications like healthcare. Its capacity for robust generalisation to unseen expert profiles and the novel integration of prior knowledge promise to improve AI-human collaborative efficacy, mitigate autonomous system errors, and lessen the demanding annotation overheads, thereby potentially widening the adoption of sophisticated AI. Conversely, negative societal considerations must be acknowledged. There exists a risk of undue reliance on such deferral systems potentially leading to a de-skilling of human experts over time, whilst poorly specified priors or inherent biases within the context data, if not appropriately managed, could result in sub-optimal deferral decisions, inadvertently perpetuating or amplifying existing biases in decision-making processes.

B Algorithms and Pseudocode

Algorithm 1 Training Expert-Agnostic Learning to Defer (EA-L2D)

Require: Expert context datasets $\{\mathcal{D}_C^E\}_{E=1}^J$, Query data \mathcal{D}_Q .

Require: Classifier h_θ (parameters θ , init. pre-trained), Rejector r_ϕ (parameters ϕ , to train).

Require: K classes, context subset size n_C , LCB param α , Batch size B .

Require: Optional: Prior parameters $\{\alpha_{k,E}^{\text{prior}}, \beta_{k,E}^{\text{prior}}\}_{k,E}$.

```

1: repeat ▷ Main training loop
2:   Sample query batch  $\mathcal{D}_Q^b = \{(\mathbf{x}_i^Q, y_i^Q)\}_{i=1}^B \subseteq \mathcal{D}_Q$ .
3:    $\mathcal{L}_{\text{batch}} \leftarrow 0$ .
4:   for each expert  $E = 1, \dots, J$  do
5:     Sample context subset  $d_E^C \subseteq \mathcal{D}_C^E$  of size  $n_C$ .
6:     Initialize  $\mathcal{R}^E = []$ . ▷ Stores  $(\mu_k^E, (\sigma_k^E)^2)$  for each class  $k$ 
7:     for each class  $k = 1, \dots, K$  do
8:       Set Beta prior  $(\alpha_k^{\text{prior}}, \beta_k^{\text{prior}})$  from optional inputs or use uninformative  $(1, 1)$  (see §4.2).
9:       Count  $n_k$  (samples of class  $k$ ) and  $t_k^E$  (expert  $E$  correct for class  $k$ ) in  $d_E^C$  (see §4.1).
10:       $\alpha_k^{\text{post}} \leftarrow \alpha_k^{\text{prior}} + t_k^E$ ;  $\beta_k^{\text{post}} \leftarrow \beta_k^{\text{prior}} + n_k - t_k^E$ .
11:       $\mu_k^E \leftarrow \frac{\alpha_k^{\text{post}}}{\alpha_k^{\text{post}} + \beta_k^{\text{post}}}$ ;  $(\sigma_k^E)^2 \leftarrow \frac{\alpha_k^{\text{post}} \beta_k^{\text{post}}}{(\alpha_k^{\text{post}} + \beta_k^{\text{post}})^2 (\alpha_k^{\text{post}} + \beta_k^{\text{post}} + 1)}$ .
12:      Append  $(\mu_k^E, (\sigma_k^E)^2)$  to  $\mathcal{R}^E$ .
13:    end for
14:     $E^* \leftarrow \arg \max_{k \in \{1..K\}} \mu_k^E$ . ▷ Expert's estimated best class from  $d_E^C$ 
15:    for each  $(\mathbf{x}^Q, y^Q)$  in  $\mathcal{D}_Q^b$  do
16:       $\mathbf{g}(\mathbf{x}^Q) \leftarrow h_\theta(\mathbf{x}^Q)$ ;  $\boldsymbol{\rho}(\mathbf{x}^Q) \leftarrow \text{softmax}(\mathbf{g}(\mathbf{x}^Q))$ .
17:       $k^* \leftarrow \arg \max_k g_k(\mathbf{x}^Q)$ ;  $\rho_{k^*} \leftarrow \rho_{k^*}(\mathbf{x}^Q)$ ;  $\rho_{E^*} \leftarrow \rho_{E^*}(\mathbf{x}^Q)$ .
18:      Extract  $\mu_{k^*}^E, (\sigma_{k^*}^E)^2, \mu_{E^*}^E, (\sigma_{E^*}^E)^2, \mu_{y^Q}^E, \sigma_{y^Q}^E$  from  $\mathcal{R}^E$  (see §4.3).
19:       $g_\perp \leftarrow r_\phi(\rho_{E^*}, \rho_{k^*}, \mu_{k^*}^E, (\sigma_{k^*}^E)^2, \mu_{E^*}^E, (\sigma_{E^*}^E)^2)$ .
20:       $w_{y^Q}^E \leftarrow \max(0, \mu_{y^Q}^E - \alpha \sigma_{y^Q}^E)$ . ▷ LCB weight, Eq. (3)
21:       $\mathcal{L}_{\text{sample}} \leftarrow \mathcal{L}_{\text{EA-LCE}}(\mathbf{g}(\mathbf{x}^Q), g_\perp, y^Q, w_{y^Q}^E, E^*)$ . ▷ EA-L2D Loss, Eq. (4)
22:       $\mathcal{L}_{\text{batch}} \leftarrow \mathcal{L}_{\text{batch}} + \mathcal{L}_{\text{sample}}$ .
23:    end for
24:  end for
25:   $\mathcal{L}_{\text{avg}} \leftarrow \mathcal{L}_{\text{batch}} / (B \times J)$ .
26:  Update parameters  $\theta, \phi$  of  $h_\theta, r_\phi$  using  $\nabla_{\theta, \phi} \mathcal{L}_{\text{avg}}$ .
27: until convergence
Ensure: Trained classifier  $h_\theta$  and rejector  $r_\phi$ .

```

C Detailed Proofs

Theorem C.1 (Hoeffding's Inequality). *Let Z_1, \dots, Z_n be random independent, identically distributed random variables, such that $0 \leq Z_i \leq 1$. Then,*

$$\Pr \left[\left| \frac{1}{n} \sum_{i=1}^n Z_i - \mathbb{E}[Z] \right| > \epsilon \right] \leq \delta = 2 \exp(-2n\epsilon^2)$$

Theorem C.2 (Boole's Inequality). *For any countable collection of events A_1, A_2, \dots, A_n in a probability space,*

$$\Pr \left(\bigcup_{i=1}^n A_i \right) \leq \sum_{i=1}^n \Pr(A_i).$$

C.1 Proof of Proposition 1

Proposition 1. *Let K be the number of classes with true class-wise expert accuracies $\bar{\theta}_k^E$, and let expert E have maximal expertise in class k^* , such that $\bar{\theta}_{k^*}^E = \max_k \bar{\theta}_k^E$ and $\bar{\theta}_{k^*}^E > \bar{\theta}_k^E$ for all $k \neq k^*$. Then, as the number of context samples grows, the predicted class converges almost surely to k^* . Moreover, if each class is observed at least n times, with*

$$n \geq \frac{\ln\left(\frac{2K}{\delta}\right)}{2\left(\frac{\Delta}{2}\right)^2}, \quad \text{where } \Delta := \bar{\theta}_{k^*}^E - \max_{k \neq k^*} \bar{\theta}_k^E,$$

then with probability at least $1 - \delta$, the posterior means satisfy $\mu_{k^}^E > \mu_k^E$ for all $k \neq k^*$; that is, the correct class is selected with high confidence.*

Proof. Step 1: Posterior convergence For each class k , the expert's true accuracy $\bar{\theta}_k^E \in [0, 1]$ is modeled with a Beta prior:

$$\theta_k^E \sim \text{Beta}(\alpha_k^E, \beta_k^E).$$

After observing n_k samples for class k , of which t_k^E are correct, the posterior becomes:

$$\theta_k^E \mid \mathcal{D}_C^E \sim \text{Beta}(\alpha_k^E + t_k^E, \beta_k^E + n_k - t_k^E),$$

with posterior mean:

$$\mu_k^E = \frac{\alpha_k^E + t_k^E}{\alpha_k^E + \beta_k^E + n_k}.$$

By the Law of Large Numbers, the empirical accuracy $\hat{\theta}_k^E := t_k^E/n_k$ converges almost surely to the true accuracy $\bar{\theta}_k^E$ as $n_k \rightarrow \infty$. Since the prior's influence vanishes in the limit, the posterior mean μ_k^E also converges almost surely to $\bar{\theta}_k^E$.

Step 2: Consistent identification of the expert class Let $k^* = \arg \max_k \bar{\theta}_k^E$ be the unique expert class. Since $\mu_k^E \xrightarrow{a.s.} \bar{\theta}_k^E$, we have:

$$\arg \max_k \mu_k^E \xrightarrow{a.s.} k^*.$$

That is, the class selected by maximising the posterior mean converges almost surely to the correct class.

Step 3: Finite-sample guarantee using Hoeffding's inequality Let $\hat{\theta}_k^E = t_k^E/n_k$ denote the empirical accuracy. We apply Hoeffding's inequality:

$$P\left(\left|\hat{\theta}_k^E - \bar{\theta}_k^E\right| \geq \epsilon\right) \leq 2 \exp(-2\epsilon^2 n_k).$$

To ensure correct identification, we require:

$$\left|\hat{\theta}_k^E - \bar{\theta}_k^E\right| < \frac{\Delta}{2}, \quad \forall k,$$

where $\Delta = \bar{\theta}_{k^*}^E - \max_{k \neq k^*} \bar{\theta}_k^E$. This guarantees:

$$\hat{\theta}_{k^*}^E > \hat{\theta}_k^E, \quad \forall k \neq k^*.$$

Setting $\epsilon = \Delta/2$ and assuming $n_k \geq n$ for all k , Hoeffding gives:

$$P\left(\exists k \text{ s.t. } \left|\hat{\theta}_k^E - \bar{\theta}_k^E\right| \geq \frac{\Delta}{2}\right) \leq 2K \exp\left(-2\left(\frac{\Delta}{2}\right)^2 n\right).$$

We want this probability $\leq \delta$, so solve:

$$2K \exp\left(-2\left(\frac{\Delta}{2}\right)^2 n\right) \leq \delta \quad \Rightarrow \quad n \geq \frac{\ln\left(\frac{2K}{\delta}\right)}{2\left(\frac{\Delta}{2}\right)^2}.$$

Thus, with this many samples per class, we have $\mu_{k^*}^E > \mu_k^E$ for all $k \neq k^*$ with probability $\geq 1 - \delta$. \square

C.2 Proof of Proposition 2

Lemma 1 (Recovery Rate from Misspecified Priors). *Let $\bar{\theta}_k^E$ be the true accuracy of expert E for class k , and suppose a potentially misspecified prior $\text{Beta}(\alpha_k^{\text{prior}}, \beta_k^{\text{prior}})$ is used. After observing n_k context samples for class k resulting in t_k^E correct predictions, the absolute error of the posterior mean estimate μ_k^E is bounded by:*

$$|\mu_k^E - \bar{\theta}_k^E| \leq \frac{S_{\text{prior}}}{S_{\text{prior}} + n_k} |\mu_{\text{prior}} - \bar{\theta}_k^E| + \frac{n_k}{S_{\text{prior}} + n_k} |\hat{\theta}_k^{(E)} - \bar{\theta}_k^E|$$

where $S_{\text{prior}} = \alpha_k^{\text{prior}} + \beta_k^{\text{prior}}$, $\mu_{\text{prior}} = \frac{\alpha_k^{\text{prior}}}{S_{\text{prior}}}$, and $\hat{\theta}_k^{(E)} = \frac{t_k^E}{n_k}$. Furthermore, as $n_k \rightarrow \infty$, the posterior mean converges to the true accuracy: $\mu_k^E \rightarrow \bar{\theta}_k^E$.

Proof. The posterior mean μ_k^E after observing t_k^E successes in n_k trials, given the prior $\text{Beta}(\alpha_k^{\text{prior}}, \beta_k^{\text{prior}})$, is:

$$\mu_k^E = \frac{\alpha_k^{\text{prior}} + t_k^E}{\alpha_k^{\text{prior}} + \beta_k^{\text{prior}} + n_k}$$

Using the definitions $S_{\text{prior}} = \alpha_k^{\text{prior}} + \beta_k^{\text{prior}}$ and $\hat{\theta}_k^{(E)} = t_k^E / n_k$, we can rewrite the posterior mean:

$$\begin{aligned} \mu_k^E &= \frac{\alpha_k^{\text{prior}} + n_k \hat{\theta}_k^{(E)}}{S_{\text{prior}} + n_k} \\ &= \frac{\alpha_k^{\text{prior}}}{S_{\text{prior}} + n_k} + \frac{n_k \hat{\theta}_k^{(E)}}{S_{\text{prior}} + n_k} \end{aligned}$$

Recalling $\mu_{\text{prior}} = \alpha_k^{\text{prior}} / S_{\text{prior}}$, we have $\alpha_k^{\text{prior}} = S_{\text{prior}} \mu_{\text{prior}}$. Substituting this gives:

$$\begin{aligned} \mu_k^E &= \frac{S_{\text{prior}} \mu_{\text{prior}}}{S_{\text{prior}} + n_k} + \frac{n_k \hat{\theta}_k^{(E)}}{S_{\text{prior}} + n_k} \\ &= \frac{S_{\text{prior}}}{S_{\text{prior}} + n_k} \mu_{\text{prior}} + \frac{n_k}{S_{\text{prior}} + n_k} \hat{\theta}_k^{(E)} \end{aligned}$$

Let $w_{\text{prior}} = \frac{S_{\text{prior}}}{S_{\text{prior}} + n_k}$ and $w_{\text{data}} = \frac{n_k}{S_{\text{prior}} + n_k}$. Note that $w_{\text{prior}} + w_{\text{data}} = 1$. Thus, the posterior mean is a weighted average of the prior mean and the empirical accuracy:

$$\mu_k^E = w_{\text{prior}} \mu_{\text{prior}} + w_{\text{data}} \hat{\theta}_k^{(E)}$$

Now consider the absolute error $|\mu_k^E - \bar{\theta}_k^E|$. Since $w_{\text{prior}} + w_{\text{data}} = 1$, we can write $\bar{\theta}_k^E = (w_{\text{prior}} + w_{\text{data}}) \bar{\theta}_k^E$.

$$\begin{aligned} |\mu_k^E - \bar{\theta}_k^E| &= |(w_{\text{prior}} \mu_{\text{prior}} + w_{\text{data}} \hat{\theta}_k^{(E)}) - (w_{\text{prior}} + w_{\text{data}}) \bar{\theta}_k^E| \\ &= |w_{\text{prior}} (\mu_{\text{prior}} - \bar{\theta}_k^E) + w_{\text{data}} (\hat{\theta}_k^{(E)} - \bar{\theta}_k^E)| \end{aligned}$$

Applying the triangle inequality ($|a + b| \leq |a| + |b|$):

$$\begin{aligned} |\mu_k^E - \bar{\theta}_k^E| &\leq |w_{\text{prior}} (\mu_{\text{prior}} - \bar{\theta}_k^E)| + |w_{\text{data}} (\hat{\theta}_k^{(E)} - \bar{\theta}_k^E)| \\ &= w_{\text{prior}} |\mu_{\text{prior}} - \bar{\theta}_k^E| + w_{\text{data}} |\hat{\theta}_k^{(E)} - \bar{\theta}_k^E| \quad (\text{since } w_{\text{prior}}, w_{\text{data}} \geq 0) \end{aligned}$$

Substituting back the definitions of w_{prior} and w_{data} yields the error bound:

$$|\mu_k^E - \bar{\theta}_k^E| \leq \frac{S_{\text{prior}}}{S_{\text{prior}} + n_k} |\mu_{\text{prior}} - \bar{\theta}_k^E| + \frac{n_k}{S_{\text{prior}} + n_k} |\hat{\theta}_k^{(E)} - \bar{\theta}_k^E|$$

This proves the first part of the proposition (i.e., bounds of the absolute error of the posterior mean estimate).

For the convergence analysis, consider the limit as $n_k \rightarrow \infty$:

$$\lim_{n_k \rightarrow \infty} w_{\text{prior}} = \lim_{n_k \rightarrow \infty} \frac{S_{\text{prior}}}{S_{\text{prior}} + n_k} = 0$$

$$\lim_{n_k \rightarrow \infty} w_{\text{data}} = \lim_{n_k \rightarrow \infty} \frac{n_k}{S_{\text{prior}} + n_k} = 1$$

By the Law of Large Numbers (specifically, the Strong Law for Bernoulli trials), the empirical accuracy converges almost surely to the true accuracy:

$$\hat{\theta}_k^{(E)} = \frac{t_k^E}{n_k} \xrightarrow{\text{a.s.}} \bar{\theta}_k^E \quad \text{as } n_k \rightarrow \infty$$

Therefore, taking the limit of the posterior mean:

$$\begin{aligned} \lim_{n_k \rightarrow \infty} \mu_k^E &= \lim_{n_k \rightarrow \infty} (w_{\text{prior}} \mu_{\text{prior}} + w_{\text{data}} \hat{\theta}_k^{(E)}) \\ &= \left(\lim_{n_k \rightarrow \infty} w_{\text{prior}} \right) \mu_{\text{prior}} + \left(\lim_{n_k \rightarrow \infty} w_{\text{data}} \right) \left(\lim_{n_k \rightarrow \infty} \hat{\theta}_k^{(E)} \right) \\ &= (0) \cdot \mu_{\text{prior}} + (1) \cdot \bar{\theta}_k^E \\ &= \bar{\theta}_k^E \end{aligned}$$

Thus, the posterior mean converges to the true accuracy regardless of the initial prior specification. \square

Proposition 2 (Sample Complexity for Overcoming Prior Misspecification). *Let $\bar{\theta}_k^E$ be the true accuracy of expert E for class k , with prior $\text{Beta}(\alpha_k^{\text{prior}}, \beta_k^{\text{prior}})$ having mean μ_{prior} and strength $S_{\text{prior}} = \alpha_k^{\text{prior}} + \beta_k^{\text{prior}}$. For any $\epsilon > 0$ and $\delta \in (0, 1)$, the number of context samples n_k needed to ensure the posterior mean μ_k^E satisfies $|\mu_k^E - \bar{\theta}_k^E| < \epsilon$ with probability at least $1 - \delta$ is bounded by:*

$$n_k \geq \max \left\{ \frac{S_{\text{prior}}(|\mu_{\text{prior}} - \bar{\theta}_k^E| - \epsilon/2)}{\epsilon/2}, \frac{2 \ln(2/\delta)}{\epsilon^2} \right\}$$

The first term accounts for overcoming prior bias (relevant if $|\mu_{\text{prior}} - \bar{\theta}_k^E| > \epsilon/2$) and the second accounts for statistical uncertainty via Hoeffding's inequality.

Proof. From Lemma 1, we have the bound:

$$|\mu_k^E - \bar{\theta}_k^E| \leq \underbrace{\frac{S_{\text{prior}}}{S_{\text{prior}} + n_k} |\mu_{\text{prior}} - \bar{\theta}_k^E|}_{\text{Term 1: Prior Bias}} + \underbrace{\frac{n_k}{S_{\text{prior}} + n_k} |\hat{\theta}_k^{(E)} - \bar{\theta}_k^E|}_{\text{Term 2: Data Estimation Error}}$$

Our objective is to find n_k such that $|\mu_k^E - \bar{\theta}_k^E| < \epsilon$ with probability at least $1 - \delta$. A sufficient condition is to ensure that each term on the right-hand side is bounded by $\epsilon/2$.

Bounding Term 1 (Prior Bias): We require:

$$\frac{S_{\text{prior}} |\mu_{\text{prior}} - \bar{\theta}_k^E|}{S_{\text{prior}} + n_k} < \frac{\epsilon}{2}$$

If $|\mu_{\text{prior}} - \bar{\theta}_k^E| \leq \epsilon/2$, the condition is trivially satisfied for the term's contribution for large enough n_k (as the fraction $\frac{S_{\text{prior}}}{S_{\text{prior}} + n_k} \rightarrow 0$). Assume $|\mu_{\text{prior}} - \bar{\theta}_k^E| > \epsilon/2$. Multiplying both sides by $(S_{\text{prior}} + n_k)$ (which is positive):

$$S_{\text{prior}} |\mu_{\text{prior}} - \bar{\theta}_k^E| < \frac{\epsilon}{2} (S_{\text{prior}} + n_k)$$

Rearranging to solve for n_k :

$$\begin{aligned} S_{\text{prior}} |\mu_{\text{prior}} - \bar{\theta}_k^E| &< \frac{\epsilon}{2} S_{\text{prior}} + \frac{\epsilon}{2} n_k \\ S_{\text{prior}} |\mu_{\text{prior}} - \bar{\theta}_k^E| - \frac{\epsilon}{2} S_{\text{prior}} &< \frac{\epsilon}{2} n_k \\ S_{\text{prior}} (|\mu_{\text{prior}} - \bar{\theta}_k^E| - \epsilon/2) &< \frac{\epsilon}{2} n_k \end{aligned}$$

Since we assumed $|\mu_{\text{prior}} - \bar{\theta}_k^E| > \epsilon/2$, the term in brackets is positive. Dividing by $\epsilon/2$:

$$n_k > \frac{S_{\text{prior}} (|\mu_{\text{prior}} - \bar{\theta}_k^E| - \epsilon/2)}{\epsilon/2}$$

Let $N_{\text{prior}}(\epsilon) = \frac{S_{\text{prior}}(|\mu_{\text{prior}} - \bar{\theta}_k^E| - \epsilon/2)}{\epsilon/2}$. We need $n_k \geq N_{\text{prior}}(\epsilon)$ (considering integer n_k).

Bounding Term 2 (Data Estimation Error): We require the contribution from this term to be less than $\epsilon/2$:

$$\frac{n_k}{S_{\text{prior}} + n_k} |\hat{\theta}_k^{(E)} - \bar{\theta}_k^E| < \frac{\epsilon}{2}$$

Since $\frac{n_k}{S_{\text{prior}} + n_k} < 1$ for $n_k > 0$, $S_{\text{prior}} \geq 2$, a sufficient condition is to ensure:

$$|\hat{\theta}_k^{(E)} - \bar{\theta}_k^E| < \frac{\epsilon}{2}$$

We want this inequality to hold with high probability. We use Hoeffding's inequality for the empirical mean of n_k independent Bernoulli trials ($\hat{\theta}_k^{(E)}$) approximating the true mean ($\bar{\theta}_k^E$):

$$\mathbb{P}(|\hat{\theta}_k^{(E)} - \bar{\theta}_k^E| \geq \eta) \leq 2e^{-2n_k\eta^2}$$

We want the probability of the undesired event ($|\hat{\theta}_k^{(E)} - \bar{\theta}_k^E| \geq \epsilon/2$) to be at most δ . Setting $\eta = \epsilon/2$:

$$\mathbb{P}(|\hat{\theta}_k^{(E)} - \bar{\theta}_k^E| \geq \epsilon/2) \leq 2e^{-2n_k(\epsilon/2)^2}$$

We require this probability to be less than or equal to δ :

$$2e^{-2n_k(\epsilon/2)^2} \leq \delta$$

Solving for n_k :

$$\begin{aligned} e^{-2n_k(\epsilon/2)^2} &\leq \frac{\delta}{2} \\ -2n_k(\epsilon/2)^2 &\leq \ln\left(\frac{\delta}{2}\right) \\ 2n_k(\epsilon/2)^2 &\geq -\ln\left(\frac{\delta}{2}\right) = \ln\left(\frac{2}{\delta}\right) \\ n_k &\geq \frac{\ln(2/\delta)}{2(\epsilon/2)^2} = \frac{2\ln(2/\delta)}{\epsilon^2} \end{aligned}$$

Let $N_{\text{data}}(\epsilon, \delta) = \frac{2\ln(2/\delta)}{\epsilon^2}$. We need $n_k \geq N_{\text{data}}(\epsilon, \delta)$.

Combining Conditions: To ensure that $|\mu_k^E - \bar{\theta}_k^E| < \epsilon$ with probability at least $1 - \delta$, we need to satisfy both the condition derived from bounding Term 1 (if applicable) and the condition derived from bounding Term 2 (probabilistically). Therefore, we require n_k to be large enough for both:

$$n_k \geq \max\{N_{\text{prior}}(\epsilon), N_{\text{data}}(\epsilon, \delta)\}$$

Substituting the expressions for $N_{\text{prior}}(\epsilon)$ and $N_{\text{data}}(\epsilon, \delta)$ gives the result stated in the proposition. The first term is considered 0 if $|\mu_{\text{prior}} - \bar{\theta}_k^E| \leq \epsilon/2$. \square

C.3 Theoretical Characterisations of EA-LCE

Proposition C.1. *Under the Beta-Binomial model of §4.1, for each class $k \in \mathcal{Y}$, as the context count $n_k \rightarrow \infty$, the posterior mean μ_k^E converges almost surely to the true expert accuracy $\bar{\theta}_k^E$ and its variance $(\sigma_k^E)^2 \rightarrow 0$. Consequently, for any fixed $\alpha \geq 0$, the LCB weight w_k^E converges almost surely to the true accuracy:*

$$w_k^E = \max\{0, \mu_k^E - \alpha \sigma_k^E\} \xrightarrow{\text{a.s.}} \bar{\theta}_k^E.$$

Proof. From §4.1, assuming a uniform prior, the posterior for the expert's unknown accuracy θ_k^E is $\text{Beta}(1 + t_k^E, 1 + n_k - t_k^E)$, where t_k^E is the number of correct predictions by expert E for class k in the context data \mathcal{D}_C^E containing n_k samples of class k . The posterior mean is $\mu_k^E = (1 + t_k^E)/(2 + n_k)$. By the Strong Law of Large Numbers, the empirical accuracy $t_k^E/n_k \xrightarrow{\text{a.s.}} \bar{\theta}_k^E$ as $n_k \rightarrow \infty$. Since the prior's influence vanishes, the posterior mean almost surely: $\mu_k^E \xrightarrow{\text{a.s.}} \bar{\theta}_k^E$. Similarly, the posterior variance $(\sigma_k^E)^2 = \frac{(1 + t_k^E)(1 + n_k - t_k^E)}{(2 + n_k)^2(3 + n_k)} \xrightarrow{\text{a.s.}} 0$. Since $\sigma_k^E = \sqrt{(\sigma_k^E)^2}$, $\sigma_k^E \xrightarrow{\text{a.s.}} 0$. Therefore, $w_k^E = \max\{0, \mu_k^E - \alpha \sigma_k^E\} \xrightarrow{\text{a.s.}} \max\{0, \bar{\theta}_k^E - \alpha \cdot 0\} = \bar{\theta}_k^E$ (since $\bar{\theta}_k^E \in [0, 1]$). \square

Theorem C.3 (Asymptotic EA-L2D Rule characterisation). *Let $R_{EA-LCE}(g)$ be the population risk associated with the EA-L2D surrogate loss $\mathcal{L}_{EA-LCE}(g; \mathbf{x}, y, \mathcal{R}_E)$ (Eq. (4), evaluated with population data). As the context counts $n_k \rightarrow \infty$ for all classes k , any minimiser g^* of R_{EA-LCE} induces the following decision rule $f^*(\mathbf{x})$:*

$$f^*(\mathbf{x}) = \begin{cases} \perp, & \text{if } \max_{y \in \mathcal{Y}} P(Y = y | X = \mathbf{x}) \leq P(Y = \bar{k} | X = \mathbf{x}) \bar{\theta}_k^E \\ \arg \max_{y \in \mathcal{Y}} g_y^*(\mathbf{x}), & \text{otherwise.} \end{cases}$$

where $\bar{k} = \arg \max_k \bar{\theta}_k^E$ is the expert's true best class, and $\bar{\theta}_k^E$ is their accuracy on that class. Furthermore, the induced classifier $h^*(\mathbf{x}) = \arg \max_{y \in \mathcal{Y}} g_y^*(\mathbf{x})$ is the Bayes-optimal multiclass predictor, $h^*(\mathbf{x}) = \arg \max_y P(Y = y | X = \mathbf{x})$.

Proof. The overall goal is to find score functions $g = (g_1, \dots, g_K, g_\perp)$ that minimise the population risk $R_{EA-LCE}(g) = \mathbb{E}_{(\mathbf{X}, Y)}[\mathcal{L}_{EA-LCE}(g; \mathbf{X}, Y, \mathcal{R}_E)]$ (a standard approach in statistical learning). To achieve this, we can equivalently minimise the conditional risk $R_{EA-LCE}(g | \mathbf{x}) = \mathbb{E}_{Y | \mathbf{X}=\mathbf{x}}[\mathcal{L}_{EA-LCE}(g; \mathbf{x}, Y, \mathcal{R}_E)]$ for each input \mathbf{x} individually. This means we want to find the scores $g(\mathbf{x})$ that perform best on average for a specific \mathbf{x} , considering all possible true labels Y according to their probabilities $P(Y = y | \mathbf{X} = \mathbf{x})$.

1. Deriving the Limiting Conditional Risk: The EA-LCE loss (Eq. (4)) for a given query input \mathbf{x}^Q , true label y^Q , and expert representation \mathcal{R}_E is:

$$\mathcal{L}_{EA-LCE}(g; \mathbf{x}^Q, y^Q, \mathcal{R}_E) = -\log P(y^Q | \mathbf{x}^Q; g) - w_{y^Q}^E \mathbb{I}[E^* = y^Q] \log P(\perp | \mathbf{x}^Q, \mathcal{R}_E; g)$$

The conditional risk for a specific \mathbf{x} is the expectation of this loss over $Y \sim P(Y | \mathbf{X} = \mathbf{x})$:

$$R_{EA-LCE}(g | \mathbf{x}) = \sum_{y' \in \mathcal{Y}} P(Y = y' | \mathbf{X} = \mathbf{x}) (-\log P(y' | \mathbf{x}; g) - w_{y'}^E \mathbb{I}[E^* = y'] \log P(\perp | \mathbf{x}, \mathcal{R}_E; g))$$

We are interested in the asymptotic case where the number of context samples $n_k \rightarrow \infty$ for all classes k . In this limit:

- From Proposition C.1, the LCB weight $w_{y'}^E$ converges to the expert's true accuracy for class y' , i.e., $w_{y'}^E \rightarrow \bar{\theta}_{y'}^E$.
- From Proposition 1, the expert's estimated best class E^* converges to their true best class, i.e., $E^* \rightarrow \bar{k} = \arg \max_k \bar{\theta}_k^E$.

Substituting these limits, the term $w_{y'}^E \mathbb{I}[E^* = y']$ converges to $\bar{\theta}_{y'}^E \mathbb{I}[\bar{k} = y']$. The conditional risk becomes:

$$\begin{aligned} \lim_{n_k \rightarrow \infty, \forall k} R_{EA-LCE}(g | \mathbf{x}) &= \sum_{y' \in \mathcal{Y}} P(Y = y' | \mathbf{X} = \mathbf{x}) (-\log P(y' | \mathbf{x}; g) - \bar{\theta}_{y'}^E \mathbb{I}[\bar{k} = y'] \log P(\perp | \mathbf{x}; g)) \\ &= \sum_{y' \in \mathcal{Y}} P(Y = y' | \mathbf{X} = \mathbf{x}) [-\log P(y' | \mathbf{x}; g)] \\ &\quad - \log P(\perp | \mathbf{x}; g) \sum_{y' \in \mathcal{Y}} P(Y = y' | \mathbf{X} = \mathbf{x}) \bar{\theta}_{y'}^E \mathbb{I}[\bar{k} = y'] \end{aligned}$$

The first sum is the expected negative log-likelihood of the classifier's predictions, $\mathbb{E}_{Y | \mathbf{X}=\mathbf{x}}[-\log P(Y | \mathbf{x}; g)]$. The second sum simplifies because $\mathbb{I}[\bar{k} = y']$ is 1 only if $y' = \bar{k}$, and 0 otherwise. So, this sum becomes $P(Y = \bar{k} | \mathbf{X} = \mathbf{x}) \bar{\theta}_{\bar{k}}^E$. Thus, the limiting conditional risk is:

$$L(g | \mathbf{x}) = \mathbb{E}_{Y | \mathbf{X}=\mathbf{x}}[-\log P(Y | \mathbf{x}; g)] - (P(Y = \bar{k} | \mathbf{X} = \mathbf{x}) \bar{\theta}_{\bar{k}}^E) \log P(\perp | \mathbf{x}; g)$$

Let $\eta_y(\mathbf{x}) = P(Y = y | X = \mathbf{x})$ be the true posterior probability of class y given \mathbf{x} . The expression can be written as:

$$L(g | \mathbf{x}) = - \sum_{y \in \mathcal{Y}} \eta_y(\mathbf{x}) \log P(y | \mathbf{x}; g) - (\eta_{\bar{k}}(\mathbf{x}) \bar{\theta}_{\bar{k}}^E) \log P(\perp | \mathbf{x}; g)$$

The model's probabilities are given by the softmax function: $P(y' | \mathbf{x}; g) = \frac{\exp(g_{y'}(\mathbf{x}))}{\sum_{y'' \in \mathcal{Y}} \exp(g_{y''}(\mathbf{x})) + \exp(g_\perp(\mathbf{x}))}$ for $y' \in \mathcal{Y} \cup \{\perp\}$. Note that in the limit, the expert representation \mathcal{R}_E (which originally parametrises g_\perp and thus $P(\perp | \cdot)$) has converged to encode the true expert accuracies $\bar{\theta}_k^E$.

2. Deriving Optimal Model Probabilities: The limiting conditional risk $L(g|\mathbf{x})$ is a form of cross-entropy loss for a $(K + 1)$ -category distribution (with categories $\mathcal{Y} \cup \{\perp\}$). To minimise this loss, we need to find scores g^* such that the model's output probabilities $P(y'|\mathbf{x}; g^*)$ align with the coefficients of the negative log terms. The scores g^* that minimize $L(g|\mathbf{x})$ will satisfy (see Appendix of Mozannar and Sontag [22] or standard derivations for multiclass logistic regression/cross-entropy loss):

$$P(y|\mathbf{x}; g^*) = \frac{\eta_y(\mathbf{x})}{\sum_{y' \in \mathcal{Y}} \eta_{y'}(\mathbf{x}) + \eta_{\bar{k}}(\mathbf{x})\bar{\theta}_{\bar{k}}^E} = \frac{\eta_y(\mathbf{x})}{1 + \eta_{\bar{k}}(\mathbf{x})\bar{\theta}_{\bar{k}}^E} \quad \text{for } y \in \mathcal{Y}$$

$$P(\perp|\mathbf{x}; g^*) = \frac{\eta_{\bar{k}}(\mathbf{x})\bar{\theta}_{\bar{k}}^E}{\sum_{y' \in \mathcal{Y}} \eta_{y'}(\mathbf{x}) + \eta_{\bar{k}}(\mathbf{x})\bar{\theta}_{\bar{k}}^E} = \frac{\eta_{\bar{k}}(\mathbf{x})\bar{\theta}_{\bar{k}}^E}{1 + \eta_{\bar{k}}(\mathbf{x})\bar{\theta}_{\bar{k}}^E}$$

From these expressions, it is clear that $P(y|\mathbf{x}; g^*) \propto \eta_y(\mathbf{x})$ for $y \in \mathcal{Y}$, and $P(\perp|\mathbf{x}; g^*) \propto \eta_{\bar{k}}(\mathbf{x})\bar{\theta}_{\bar{k}}^E$.

3. Induced Classifier is Bayes-Optimal: The system's classifier $h^*(\mathbf{x})$ chooses the class $y \in \mathcal{Y}$ that maximises the score $g_y^*(\mathbf{x})$. Since the softmax function $P(y|\mathbf{x}; g^*) = \exp(g_y^*(\mathbf{x})) / (\sum \exp(\cdot))$ is monotonic with respect to $g_y^*(\mathbf{x})$ (for a fixed denominator), maximising $g_y^*(\mathbf{x})$ is equivalent to maximising $P(y|\mathbf{x}; g^*)$. Given $P(y|\mathbf{x}; g^*) = \eta_y(\mathbf{x}) / (1 + \eta_{\bar{k}}(\mathbf{x})\bar{\theta}_{\bar{k}}^E)$, maximising this term is equivalent to maximising $\eta_y(\mathbf{x})$ because the denominator is a positive constant for a given \mathbf{x} and expert. Therefore, $h^*(\mathbf{x}) = \arg \max_{y \in \mathcal{Y}} \eta_y(\mathbf{x}) = \arg \max_{y \in \mathcal{Y}} P(Y = y|X = \mathbf{x})$. This is (by definition) the Bayes-optimal multiclass classifier.

4. Deferral Rule: The system defers if the score for deferral $g_{\perp}^*(\mathbf{x})$ is greater than or equal to the score of any class, i.e., $g_{\perp}^*(\mathbf{x}) \geq \max_{y \in \mathcal{Y}} g_y^*(\mathbf{x})$. Again, due to the monotonicity of the softmax function, this condition is equivalent to comparing the corresponding probabilities:

$$P(\perp|\mathbf{x}; g^*) \geq \max_{y \in \mathcal{Y}} P(y|\mathbf{x}; g^*)$$

Substituting the optimal probabilities derived in Step 2:

$$\frac{\eta_{\bar{k}}(\mathbf{x})\bar{\theta}_{\bar{k}}^E}{1 + \eta_{\bar{k}}(\mathbf{x})\bar{\theta}_{\bar{k}}^E} \geq \max_{y \in \mathcal{Y}} \left(\frac{\eta_y(\mathbf{x})}{1 + \eta_{\bar{k}}(\mathbf{x})\bar{\theta}_{\bar{k}}^E} \right)$$

Since the denominator $(1 + \eta_{\bar{k}}(\mathbf{x})\bar{\theta}_{\bar{k}}^E)$ is positive (as probabilities η and true accuracies $\bar{\theta}$ are non-negative), we can multiply both sides by it:

$$\eta_{\bar{k}}(\mathbf{x})\bar{\theta}_{\bar{k}}^E \geq \max_{y \in \mathcal{Y}} \eta_y(\mathbf{x})$$

Substituting back $\eta_y(\mathbf{x}) = P(Y = y|X = \mathbf{x})$:

$$P(Y = \bar{k}|X = \mathbf{x})\bar{\theta}_{\bar{k}}^E \geq \max_{y \in \mathcal{Y}} P(Y = y|X = \mathbf{x})$$

This establishes the deferral condition. Combined with the classifier's decision when not deferring, this defines the optimal decision rule $f^*(\mathbf{x})$ as stated in the theorem. \square

Remark C.1 (Interpretation of the Asymptotic Rule). *Theorem C.3 shows that EA-L2D learns a system that asymptotically implements the standard Bayes classifier $h^*(\mathbf{x}) = \arg \max_y P(Y = y|X = \mathbf{x})$. However, its deferral rule is different from the standard L2D Bayes-optimal rule derived from the 0-1 loss. The standard rule (e.g., from Mozannar and Sontag [22]) defers if $\max_y P(Y = y|X = \mathbf{x}) \leq \mathbb{E}_{Y|\mathbf{x}}[\bar{\theta}_Y^E] = \sum_y P(Y = y|X = \mathbf{x})\bar{\theta}_y^E$, where $\bar{\theta}_Y^E$ represents the expert's accuracy if the true class is Y .*

The EA-L2D rule, in contrast, defers if $\max_y P(Y = y|X = \mathbf{x}) \leq P(Y = \bar{k}|X = \mathbf{x})\bar{\theta}_{\bar{k}}^E$. This distinct deferral rule, focused on the expert's single best class \bar{k} and their performance on it ($\bar{\theta}_{\bar{k}}^E$), arises directly from the structure of the \mathcal{L}_{EA-LCE} surrogate. The deferral component of the loss, $-w_{y^Q}^E \mathbb{I}[E^ = y^Q] \log P(\perp|\cdot)$, specifically rewards deferral when the true class y^Q aligns with the expert's (asymptotically true) best class \bar{k} , and the expert's performance $w_{y^Q}^E$ (asymptotically $\bar{\theta}_{y^Q=\bar{k}}^E$) on that class is high. This encourages deferral primarily based on the expert's peak competence area, rather than their average performance across all classes weighted by their likelihood.*

D Experimental Details

Computational Resources All experiments in this paper were ran using a NVIDIA GeForce RTX 4090 GPU, AMD Ryzen 9 7950X 16-Core Processor and 64GB DDR5 RAM.

Classifier Models The classifier architecture varies by dataset: ResNet-34 [31] for **HAM10000**, and a pretrained EfficientNet B0 [32] **Liver Tumours** and **Retinal OCT**, and MobileNetV2 [33] for **Blood Cells**.

Rejector Model For all experimental models, we keep the architecture of the rejector constant. For this, we utilise a 6-layer MLP with hidden-dimensionality of 256.

Training Details Details on number of ID/OOD experts, context set sizes N_C^E and n_C^E are provided in Table 1. We utilise training and validation batch sizes of 128 for all datasets. We utilise the Adam optimiser [34] for all experiments, with a learning rate of 0.001 for **Liver Tumours** and **HAM10000**, 0.0001 **Retinal OCT** and 0.0005 for **Blood Cells**. All models are trained until convergence, measured via early stopping on the validation set measuring AURSAC (patience 50). We utilise a standard $\alpha = 1$ hyperparameter for the LCB-weighted loss for all experiments.

E Pop-Avg Baseline Details

Following Tailor et al. [2], we consider a baseline that models the average expert using their predictions on query data. Unlike Tailor et al. [2], who incorporate the deferral component of the loss for every data point and weight it based on the population of expert accuracies, we compute the average prediction as the *mode* of the expert predictions for each query data point. Additionally, we only incorporate the deferral component when the mode response matches the ground-truth label (similar to \mathcal{L}_{CE}). This baseline serves as an initial inference method for multi-expert L2D scenarios, particularly for cases with unseen experts at test time, enabling a natural baseline for a direct comparison with L2D-Pop and EA-L2D.

$$\mathcal{L}_{CE}(g_1, \dots, g_K, g_{\perp}; \mathbf{x}^Q, y^Q, \{m_E^Q\}_{e=1}^E) = -\log \left(\frac{\exp \{g_y(\mathbf{x})\}}{\sum_{y' \in \mathcal{Y} \cup \perp} \exp \{g_{y'}(\mathbf{x})\}} \right) - \mathbb{I}[\mathcal{M} = y] \log \left(\frac{\exp \{g_{\perp}(\mathbf{x})\}}{\sum_{y' \in \mathcal{Y} \cup \perp} \exp \{g_{y'}(\mathbf{x})\}} \right).$$

where $\mathcal{M} = \text{Mode}(\{m_E^Q\}_{e=1}^E)$.

F Additional Experiments

F.1 RQ3: Impact of Prior Knowledge and Context Data Interaction

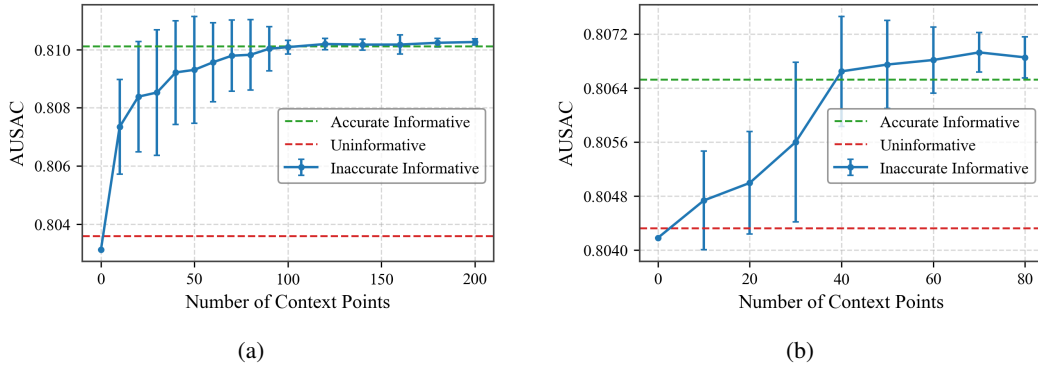


Figure 6: AURSAC performance under different prior conditions across context points.

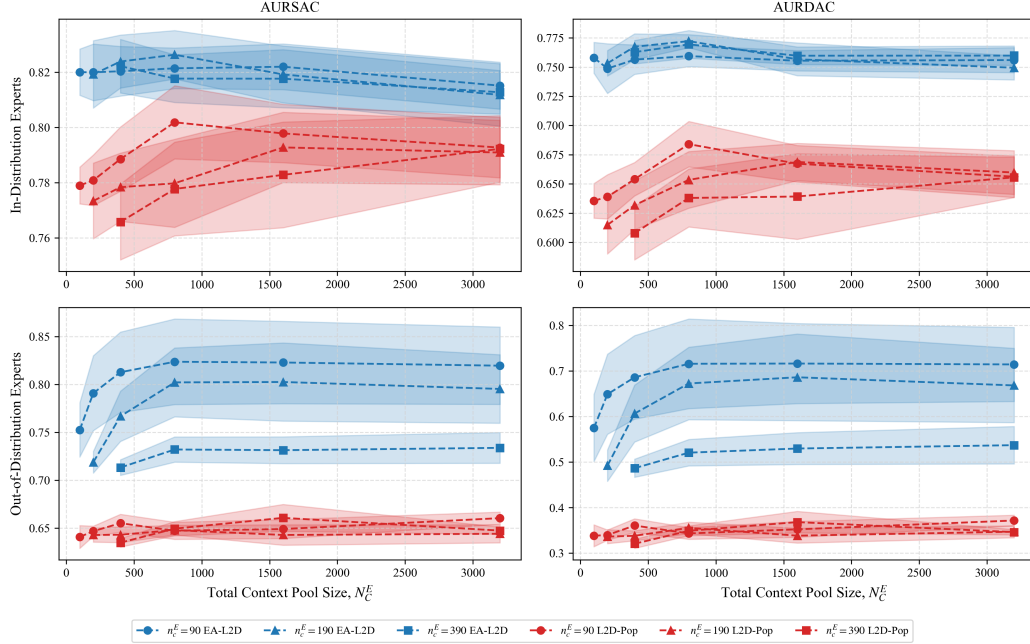


Figure 7: Performance (AURSAC, AURDAC) of EA-L2D and L2D-Pop on the **Blood Cells** dataset ($p = 0.2$) versus total expert context pool size (N_C^E). Curves show varying sampled context sizes (n_C^E) for In-Distribution (ID, top row) and Out-of-Distribution (OOD, bottom row) experts.

F.2 RQ4: Performance Scaling with Expert Context Data

To investigate how performance scales with the amount of expert context data, we conduct an experiment on the **Blood Cells** dataset. We vary both the number of context predictions sampled to construct an expert’s representation, n_C^E , and the total size of the pool from which these predictions are drawn, N_C^E . This analysis is performed for EA-L2D and L2D-Pop, measuring AURSAC and AURDAC for ID and OOD experts. All experiments in this subsection maintain a high expert diversity setting ($p = 0.2$). Fig. 7 visualises these results.

Findings: For EA-L2D, OOD performance (AURSAC and AURDAC) generally improves with an increasing total context pool N_C^E , plateauing or slightly diminishing beyond an optimal pool size (e.g., $N_C^E \approx 800 - 1600$ for $n_C^E = 90$). However, increasing the sampled context n_C^E from a fixed, sufficiently large N_C^E does not consistently enhance, and can sometimes degrade, OOD performance; for instance, with $N_C^E = 800$, $n_C^E = 90$ (AURSAC OOD: 0.824) outperforms $n_C^E = 190$ (AURSAC OOD: 0.802). In contrast, L2D-Pop’s performance, particularly for OOD experts, exhibits less sensitivity to variations in either N_C^E or n_C^E . Across all configurations, EA-L2D consistently achieves superior AURSAC and AURDAC for OOD experts compared to L2D-Pop (e.g., at $n_C^E = 90$, $N_C^E = 800$, EA-L2D’s AURSAC OOD of 0.824 versus L2D-Pop’s 0.647). This highlights EA-L2D’s more effective use of context data for robust OOD generalisation.

F.3 RQ5: How robust is EA-L2D’s performance compared to L2D-Pop when faced with input distribution shift?

To address RQ5, we simulate ten cohorts comprising both ID and OOD experts. EA-L2D and L2D-Pop are trained on the **HAM10000** dataset using only the ID experts. We then assess the robustness of each method by evaluating the performance of both ID and OOD experts on the BCN20000 dataset [35], which serves as the OOD input data benchmark.

The **BCN2000** dataset is a large-scale dataset of dermoscopic images with over 20,000 images across 7 categories, of which 6 match up with the HAM10000 categories (actinic keratoses and intraepithelial carcinoma / Bowen’s disease (akiec), basal cell carcinoma (bcc), benign keratosis-like lesions (solar lentigines / seborrheic keratoses and lichen-planus like keratoses, bkl), dermatofibroma (df),

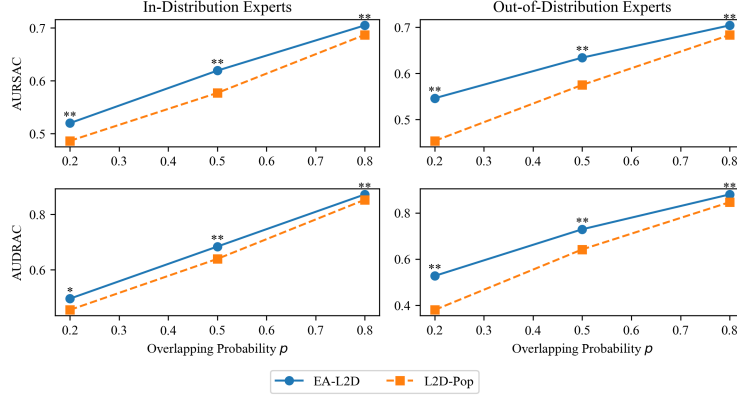


Figure 8: Robustness to input distribution shift: AURSAC and AURDAC comparison. Performance of EA-L2D and L2D-Pop when trained on **HAM10000** (with ID experts) and evaluated on the **BCN20000** dataset (OOD input data). Results are presented for scenarios with in-distribution (ID) and out-of-distribution (OOD) expert types, across varying expert diversity levels ($p \in \{0.2, 0.5, 0.8\}$). Curves illustrate average performance over ten simulated expert cohorts for each condition. Asterisks denote statistical significance in favour of EA-L2D: * for $p < 0.1$ and ** for $p < 0.05$ (via two-tailed paired samples t-test).

melanoma (mel), melanocytic nevi (nv) and vascular lesions (angiomas, angiokeratomas, pyogenic granulomas and hemorrhage, vasc). However, the 7th category, keratoacanthoma, is not present in **HAM10000**. We remove this category from the BCN 2000 dataset for consistency. The BCN dataset represents a significant distribution shift from **HAM10000** primarily because it was collected "in the wild" from multiple clinical centers in Spain, whereas **HAM10000** was collected in a more controlled setting in Austria. This results in greater diversity in imaging conditions (different devices, lighting, angles), patient demographics (varying skin types and sun exposure patterns), and clinical practices. While both datasets share similar diagnostic categories, these fundamental differences in data collection and population characteristics create meaningful shifts in both the input space (image characteristics) and the relationship between features and labels, making it an excellent test for model robustness.

Findings: Evaluation on the **BCN20000** dataset, an input distribution significantly shifted from **HAM10000** training data, confirms EA-L2D’s superior robustness over L2D-Pop (Figure 8). EA-L2D consistently achieved statistically significant ($p \leq 0.008$) improvements in both AURSAC and AURDAC across all expert types (ID/OOD) and diversity levels ($p \in \{0.2, 0.5, 0.8\}$).

As expected, EA-L2D’s advantage was most prominent for OOD experts facing this input shift, particularly with high specialisation ($p = 0.2$). Here, EA-L2D improved AURSAC to 0.546 (vs. L2D-Pop’s 0.454) and AURDAC to 0.527 (vs. 0.380). This highlights EA-L2D’s enhanced ability to maintain accuracy and defer effectively under combined input and expert novelty. While higher expert skill overlap (larger p) improved both methods, EA-L2D maintained its significant lead (e.g., OOD experts, $p = 0.8$: AURSAC 0.704 vs. 0.683; AURDAC 0.880 vs. 0.847).

Notably, on **BCN20000**, EA-L2D often performed as well or better with OOD expert types than ID ones. L2D-Pop, conversely, showed more pronounced degradation for OOD experts, especially in AURDAC with specialised experts. These results highlight that EA-L2D’s expert-agnostic mechanism, using constructed statistical representations, offers greater resilience to both expert variations and substantial input distribution shifts.

F.4 Ablation Study: Impact of LCB Weighting in EA-L2D Loss

To examine the contribution of the uncertainty-aware Lower Confidence Bound (LCB) weighting in our EA-L2D loss (Eq. (4)), we conducted an ablation study on the **HAM10000** dataset. This study aimed to assess how well our proposed LCB weighting enables the system to make careful deferral decisions, especially when expert performance is uncertain due to limited context data.

Table 3: Performance of LCB weighting ablations on HAM10000 (mean \pm std.dev. over 8 seeds). AURSAC and AURDAC evaluated over (0,1). AURDAC Cond. refers to AURDAC conditioned on deferral to the specified true expert type (HS: High-Skill, MS: Medium-Skill, LS: Low-Skill; HU: High-Uncertainty, MU: Medium-Uncertainty, LU: Low-Uncertainty). Best result per column (excluding Classifier_Only for deferral metrics) is in **bold**. * indicates $p < 0.05$ in a paired t-test vs LCB_Full.

Ablation Condition	AURSAC (Overall)	AURDAC (Overall)	AURDAC Conditional (True Expert Type)				
			HS-HU	HS-MU	LS-HU	MS-HU	OL-LU
LCB_Full	0.6206 \pm 0.0063	0.3517 \pm 0.0159	0.3988 \pm 0.0386	0.4568 \pm 0.0383	0.1517 \pm 0.0239	0.3768 \pm 0.0380	0.3439 \pm 0.0332
LCB_Mean_Only	0.6152 \pm 0.0085	0.3418 \pm 0.0181	0.4016 \pm 0.0404	0.4561 \pm 0.0398	0.1258 \pm 0.0268*	0.3621 \pm 0.0408	0.3471 \pm 0.0333
LCB_Binary_Specialty	0.6130 \pm 0.0050*	0.3385 \pm 0.0147	0.3934 \pm 0.0595	0.4606 \pm 0.0419	0.1297 \pm 0.0285	0.3581 \pm 0.0391	0.3419 \pm 0.0285
Classifier_Only	0.6009 \pm 0.0069	0.2522 \pm 0.0136	0.3267 \pm 0.0316	0.2983 \pm 0.0456	0.1288 \pm 0.0260	0.3545 \pm 0.0432	0.1481 \pm 0.0358

We simulated five distinct types of experts to create a challenging evaluation environment where uncertainty plays a critical role:

1. **HS-HU (High-Skill, High-Uncertainty)**: High true accuracy (0.90 expertise / 0.20 other), very few context samples (2/1), leading to high uncertainty.
2. **MS-HU (Medium-Skill, High-Uncertainty)**: Moderate true accuracy (0.60/0.30), very few context samples (2/1), causing high uncertainty.
3. **LS-HU (Low-Skill, High-Uncertainty “Lucky”)**: Low true accuracy (0.30/0.10), very few context samples (2/1). These experts are critical as they might incorrectly appear competent if their limited context samples are correct by chance.
4. **HS-MU (High-Skill, Medium-Uncertainty)**: High true accuracy (0.90/0.20), more context samples (10/3), leading to medium uncertainty; this group serves as a control.
5. **OL-LU (Oracle-Like, Low-Uncertainty)**: Very high true accuracy (0.99/0.05), many context samples (20/5), resulting in low uncertainty.

We compared four EA-L2D loss variants using these experts, averaged over 8 seeds, with $\alpha = 1.0$ for LCB_Full:

6. LCB_Full: Our proposed method, $w_{y^Q}^E = \max(0, \mu_{k=y^Q}^E - \alpha \sigma_{k=y^Q}^E)$.
7. LCB_Mean_Only: Uses only the mean, $w_{y^Q}^E = \mu_{k=y^Q}^E$ (equivalent to $\alpha = 0$).
8. LCB_Binary_Specialty: A simpler weighting, $w_{y^Q}^E = 1.0$ if $E^* = y^Q$, 0 otherwise.
9. Classifier_Only: A baseline that never defers. Here, AURDAC metrics represent the performance of randomly assigned experts, as this baseline makes no actual deferrals.

Hypotheses Based on Design Principles:

- (i) We anticipated that LCB_Full would achieve strong overall performance (AURSAC and AURDAC).
- (ii) We expected that LCB_Full, by penalising high uncertainty ($\sigma_{k=y^Q}^E$), would be significantly more resilient to misleading estimates from “lucky” LS-HU experts compared to LCB_Mean_Only.
- (iii) We hypothesised that LCB_Full would enable more nuanced deferral than LCB_Binary_Specialty.

Findings: The detailed results, including statistical significance markers ($p < 0.05$) from paired t-tests comparing against LCB_Full, are presented in Table 3. Our proposed LCB_Full method achieved the best overall performance, yielding the highest mean AURSAC (0.6206 \pm 0.0063) and AURDAC Overall (0.3517 \pm 0.0159). It significantly outperformed LCB_Binary_Specialty on AURSAC, supporting hypothesis (i). All deferral methods significantly surpassed the Classifier_Only baseline.

In particular, the results for the LS-HU (Low-Skill, High-Uncertainty) experts now strongly support hypothesis (ii). LCB_Full achieved the highest conditional AURDAC for this group (0.1517 \pm 0.0239), significantly outperforming LCB_Mean_Only (0.1258 \pm 0.0268). This demonstrates that explicitly incorporating the uncertainty $\sigma_{k=y^Q}^E$ via the LCB term makes LCB_Full more robust to potentially misleadingly high mean accuracy estimates derived from sparse context for low-skill experts. It successfully avoids deferring inappropriately to these “lucky” experts compared to the uncertainty-agnostic LCB_Mean_Only variant.

For other expert types, performance was generally comparable across the LCB variants. `LCB_Full` performed best for HS-HU and MS-HU experts, while other methods showed slight (but not statistically significant vs `LCB_Full`) advantages for HS-MU and OL-LU experts.

In conclusion, the LCB weighting in EA-L2D provides a tangible benefit for robust deferral. It leads to the best overall system and deferral accuracy, and critically, it significantly improves the quality of deferral decisions involving low-skill experts whose competence might be overestimated due to high uncertainty from limited data. While simpler approaches can be competitive in less ambiguous scenarios, `LCB_Full`'s uncertainty awareness provides a valuable safeguard, enhancing the reliability required for practical L2D systems.

G Datasets

We used five public medical imaging datasets to develop and test our methods. Each dataset is described below, noting its contents and license.

HAM10000 Dataset The HAM10000 dataset [23] contains 10,015 dermoscopic images of common pigmented skin lesions. It was created to provide a larger, more varied resource for training systems to identify skin conditions. Images were collected over twenty years from Vienna, Austria, and Queensland, Australia. The dataset covers seven diagnostic types: melanocytic nevi, melanoma, benign keratosis-like lesions, basal cell carcinoma, actinic keratoses, vascular lesions, and dermatofibroma. Over half the diagnoses were confirmed by histopathology, with the rest checked by follow-up, expert review, or confocal microscopy. The dataset is available via the Harvard Dataverse. The original paper states the license is Creative Commons Attribution 4.0 International (CC BY 4.0).

Blood Cells Dataset The Blood Cells dataset [24], has 17,092 microscope images of single normal blood cells. It was made to help build and test systems for recognising blood cells, particularly using deep learning. The images are 360x363 pixel JPGs, taken with a CellaVision DM96 machine at the Hospital Clinic of Barcelona. Expert pathologists labelled the cells. The dataset groups cells into eight types: neutrophils, eosinophils, basophils, lymphocytes, monocytes, immature granulocytes, erythroblasts, and platelets. Immature granulocytes are grouped together because individually identifying them is less clinically important and difficult even for experts. This grouping focuses on clearer categories for model training. The dataset is on Mendeley Data and uses the Creative Commons Attribution 4.0 International (CC BY 4.0) license.

Retinal OCT Dataset The Retinal OCT dataset [25], provides a large set of images for studying retinal diseases. A common version contains 84,484 OCT images. Images fall into four classes: Choroidal Neovascularization (CNV), Diabetic Macular Edema (DME), Drusen, and Normal scans. This large size reflects the common use of OCT and the time needed to check scans manually. Images were checked carefully: first for quality, then graded independently by trained staff and doctors, and finally verified by senior specialists. This detailed checking helps make the dataset reliable for training machine learning models. The dataset is publicly available on Mendeley Data) Platforms hosting the data indicate it is licensed under Creative Commons Attribution 4.0 International (CC BY 4.0).

Liver Tumours (LiTS) Dataset: Liver Tumours The Liver Tumour Segmentation (LiTS) dataset [26] (referenced as "Liver Tumours" in this paper) is a resource for testing liver and liver tumour segmentation methods. It includes 131 CT volumes for training and 70 for testing. Data came from seven hospitals and research centres, offering varied clinical cases. The dataset includes different tumour types, sizes, looks, and contrast levels, making it a tough, realistic test. The LiTS dataset and its online testing system are on CodaLab. It uses the Creative Commons Attribution-NonCommercial-NoDerivatives 4.0 International (CC BY-NC-ND 4.0) license.

G.1 BCN20000 Dataset

The BCN20000 dataset [35], contains 18,946 dermoscopic images. Images were collected at the Hospital Clínic in Barcelona, Spain, from 2010 to 2016. The dataset aims to help research in classifying dermoscopic images of skin cancer without strict limits. It includes difficult cases like lesions on nails or mucosa, large lesions, and pale ones. It covers eight main diagnostic types. The test set also has a ninth class for lesions that did not fit the main types. The data paper is in Scientific

Data. BCN20000 is available under the Creative Commons Attribution 4.0 International (CC BY 4.0) license.